Early season mesopelagic carbon remineralization and transfer efficiency in the naturally iron-fertilized Kerguelen area

Jacquet S.H.M.[1], F. Dehairs[2], D. Lefèvre[1], A.J. Cavagna[2], F. Planchon[3], U. Christaki[4], L. Monin[5], L. André[5], I. Closset[6] and D. Cardinal[6]

[1]Aix Marseille Université, CNRS/INSU, IRD, Mediterranean Institute of Oceanography (MIO), UM 110, 13288 Marseille, France

[2]Vrije Universiteit Brussel, Analytical, Environmental & Geo-Chemistry and Earth System Sciences, Brussels, Belgium

[3]Laboratoire des Sciences de l'Environnement Marin (LEMAR), Université de Brest, CNRS, IRD, UMR 6539, IUEM; Technopôle Brest Iroise, Place Nicolas Copernic, F-29280 Plouzané, France

[4]INSU-CNRS, UMR8187 LOG, Laboratoire d'Océanologie et de Géosciences, Université du Littoral Côte d'Opale, ULCO, 32 avenue Foch, 62930 Wimereux, France

[5]Earth Sciences Department, Royal Museum for Central Africa, Leuvensesteenweg 13, Tervuren, B 3080, Belgium

[6]Sorbonne Universités (UPMC, Univ Paris 06)-CNRS-IRD-MNHN, LOCEAN Laboratory, 4 place Jussieu, F-75005 Paris, France

Corresponding author: stephanie.jacquet@mio.osupytheas.fr

Abstract

We report on the zonal variability of mesopelagic particulate organic carbon remineralization and deep carbon transfer potential during the Kerguelen Ocean and Plateau compared Study 2 expedition (KEOPS 2; Oct.-Nov. 2011) in an area of the Polar Front supporting recurrent massive blooms from natural Fe fertilization. Mesopelagic carbon remineralization (MR) was assessed using the excess, non-lithogenic particulate barium (Ba_{xs}) inventories in mesopelagic waters and compared with bacterial production (BP), surface primary production (PP) and export production (EP). Results for this early season study are compared with results obtained during a previous study (2005; KEOPS 1) for the same area at a later stage of the phytoplankton bloom. Our results reveal the patchiness of the season advancement and of the establishment of remineralization processes between plateau (A3) and Polar Front sites during KEOPS 2. For the Kerguelen plateau (A3 site) we observe a similar functioning of the mesopelagic ecosystem during both seasons (spring and summer), with low and rather stable remineralization fluxes in the mesopelagic column (150-400 m). The shallow water column (~500m), the lateral advection, the zooplankton grazing pressure and the pulsed nature of the POC transfer at A3 seem to drive the extend of MR processes on the plateau. For deeper stations (>2000 m) located on the margin, inside a Polar Front meander, as well as in the vicinity of the Polar Front, east of Kerguelen, remineralization in the upper 400 m in general represents a larger part of surface carbon export, but when considering the upper 800 m, in some cases, the entire flux of exported carbon is remineralized. In the Polar Front meander, where successive stations form a time series, two successive events of particle transfer were evidenced by remineralization rates: a first mesopelagic and deep transfer from a past bloom before the cruise, and a second transfer expanding at mesopelagic layers during the cruise. Regarding the deep carbon transfer

efficiency, it appeared that above the plateau (A3 site) the mesopelagic remineralization was not a major barrier to the transfer of organic matter to the sea-floor (close to 500 m). There the efficiency of carbon transfer to the bottom waters (>400 m) as assessed by PP, EP and MR fluxes comparisons reached up to 87% of the carbon exported from the upper 150 m. In contrast, at the deeper locations mesopelagic remineralization clearly limited the transfer of carbon to depths >400 m. For sites at the margin of the plateau (station E-4W) and the Polar front (station F-L), mesopelagic remineralization even exceeded upper 150 m export, resulting in a null transfer efficiency to depths >800 m. In the Polar Front meander (time series), the capacity of the meander to transfer carbon to depth >800 m was highly variable (0 to 73 %). The highest carbon transfer efficiencies in the meander are furthermore coupled to intense and complete deep (>800 m) remineralization, resulting again in a close to zero deep (>2000 m) carbon sequestration efficiency there.

Key Words: particulate barium, mesopelagic carbon remineralization, carbon transfer efficiency, Southern Ocean

77 **1. INTRODUCTION**

78 While numerous artificial (Boyd et al., 2000, 2004; Gervais et al.,
79 2002; Buesseler et al., 2004, 2005; de Baar et al., 2005; Hoffmann et al.,
80 2006; Boyd et al., 2012; Smetacek et al., 2012) and natural (Blain et al.,
81 2007; Pollard et al., 2009; Zhou et al., 2010, 2013) ocean iron-fertilization
82 experiments in the Southern Ocean demonstrated the role of iron in
83 enhancing the phytoplankton biomass and production in high-nutrient low-
84 chlorophyll (HNLC) regions, determining to what extent fertilization could
85 modify the transfer of particulate organic carbon (POC) to the deep ocean is
86 far from being comprehensively achieved (Lampitt et al., 2008; Morris and
87 Charette, 2013; Le Moigne et al., 2014; Robinson et al., 2014). This is partly
88 due to the short term over which the observations were made, precluding
89 extrapolation to longer time scales. Moreover, when assessing whether Fe-
90 supply could induce vertical POC transfer, the magnitude of the export from
91 surface is not the only important parameter to take into account. Indeed, POC
92 fate in the mesopelagic zone (defined as 100-1000 m depth layer) is often
93 largely overlooked although these depth layers are responsible for the
94 remineralization of most of the POC exported from the surface layer (Martin et
95 al., 1987; Longhurst, 1990; Lampitt and Antia, 1997; François et al., 2002;
96 Buesseler et al., 2007b; Buesseler and Boyd, 2009). Only few studies
97 considered mesopelagic carbon (C) remineralization rates (Buesseler et al.,
98 2007a; Jacquet et al., 2008a, 2008b, 2011a, 2011b; Salter et al., 2007) to
99 estimate the response of deep POC export to fertilization. Assessing
100 mesopelagic C remineralization is pivotal to evaluate remineralization length
101 scale as well as the time scale of the C storage in the deep ocean. Indeed the
102 typical depth of the main thermocline, 1000 m (IPCC, WG1, 2007, chp5) is
103 often referred to as the horizon clearly removed from the surface ocean and
104 atmosphere (Passow and Carlson, 2012). Overall, assessing mesopelagic C
105 remineralization will allow to better quantify the ocean's biological carbon

106 pump and its efficiency in the global C cycle which bears large uncertainty and
107 is currently under debate (e.g. from 5 Gt/yr in Henson et al., 2011 to 21 Gt
108 C/yr in Laws et al., 2000 and 13 Gt/yr in IPPC WG1 report (ch. 6, 2013).
109 The present work aims at understanding the impact of a natural iron-
110 induced bloom on the mesopelagic POC remineralization and zonal variability
111 in the Kerguelen area (Southern Ocean). Here, C remineralization was
112 assessed from particulate biogenic Ba (hereafter called excess-Ba or Ba_{xs};
113 mainly forms as barite $BaSO_4$ crystals) contents in the mesopelagic water
114 column. The link between barite and C remineralization resides in the fact that
115 this mineral precipitates inside oversaturated micro-environments (biogenic
116 aggregates) during the process of prokaryotic degradation of sinking POC
117 (Dehairs et al., 1980, 1992, 1997, 2008; Stroobants et al., 1991, Cardinal et
118 al., 2001, 2005; Jacquet et al., 2007, 2008b, 2011a; Planchon et al., 2013;
119 Sternberg et al. 2007, 2008a, 2008b). Once the aggregates have been
120 remineralized, barites are released and spread over the mesopelagic layer.
121 Overall, earlier work highlights the fact that suspended barite in mesopelagic
122 waters builds up over the growing season and reflects past remineralization
123 activity integrated over several days to weeks (Dehairs et al., 1997; Cardinal
124 et al., 2005; Jacquet et al., 2007, 2008b). An algorithm relating mesopelagic
125 Ba_{xs} contents to oxygen consumption (Shopova et al., 1995; Dehairs et al.,
126 1997) allowed remineralization of POC fluxes to be estimated for the
127 mesopelagic layer. Combined with surface C production and export estimates,
128 mesopelagic Ba_{xs} also informs on the efficiency of the system toward deep
129 carbon transfer. From earlier studies, the efficiency of C transfer through the
130 mesopelagic layer was reported to increase under artificially induced (EIFEX;
131 Strass et al., 2005; Smetacek et al., 2012) and natural (KEOPS; Blain et al.,
132 2007) Fe-replete conditions (Jacquet et al., 2008a, 2008b; Savoye et al.,
133 2008) compared to Fe-limited, non-bloom, HNLC reference stations in the
134 Southern Ocean. In contrast, C transfer efficiency through the mesopelagic

135 layer was reported smaller in natural Fe-replete locations during the SAZ-
136 Sense cruise off Tasmania (Jacquet et al., 2011a, 2011b). Differences in
137 plankton community structure and composition (e.g. diatoms vs. flagellates,
138 type of diatoms) were pointed at, as possible causes of such discrepancies in
139 C transfer efficiency through the mesopelagic layer (Jacquet et al., 2008a,
140 2011a, 2011b). Also, differences in integration time scales for the processes
141 that control the carbon fluxes in artificially vs. naturally Fe fertilized systems,
142 may yield an incomplete picture of the C transfer potential and lead to
143 misleading conclusions.

144 Here, we examine changes in mesopelagic POC remineralization
145 during the early spring (Oct. –Nov. 2011) KEOPS 2 expedition to the naturally
146 iron fertilized area eastward of Kerguelen Islands. The hydrographic structure
147 of the Kerguelen area generates contrasted environments that are differently
148 impacted by iron availability and mesoscale activity. The specific objectives of
149 the present work are to assess the zonal variability of mesopelagic C
150 remineralization and deep C transfer potential, and to identify possible causes
151 inducing this variability. As the same area was visited earlier in 2005 during
152 summer at a late stage of the bloom (KEOPS 1; Jan.-Feb., 2005), this
153 condition offers a unique opportunity to estimate the main carbon fluxes over
154 most of the growth season. Mesopelagic C remineralization estimates are
155 compared to particle and biological parameters as reported in other papers
156 included in this issue (Cavagna et al., 2014; Christaki et al., 2014; Dehairs et
157 al., 2014; Lasbleiz et al., 2014; Laurenceau-Cornec et al., 2014; Planchon et
158 al., 2014; Van der Merve et al., 2015) and in Blain et al., (2007); Christaki et
159 al. (2008); Jacquet et al., (2008a); Park et al., (2008); Savoye et al., (2008).
160

161 **2. EXPERIMENT AND METHODS**

162 **2.1. Study area**

The KEOPS 2 (Kerguelen Ocean and Plateau compared Study) cruise was conducted in austral spring at the onset of the bloom from 10 October to 20 November aboard the R/V *Marion Dufresne* (TAAF/IPEV). The KEOPS 2 expedition studied the Kerguelen Plateau area (Indian sector of the Southern Ocean) which is characterized by the passage of the Polar Front (PF), as illustrated in Fig.1a. The Kerguelen Plateau is surrounded by the Antarctic Circumpolar Current (ACC) whose main branch circulates to the north of the plateau (Park et al., 2008). A second branch of the ACC circulates to the south of Kerguelen Islands to further join a branch of the Fawn Trough Current (FTC). The FTC has a main northeast direction, but a minor branch splits away northwestward to join the eastern side of the Kerguelen plateau (Park et al., 2008; Fig1.a). These particular hydrographic features generate a mosaic of recurrent massive bloom patterns in the northeastern part of the Plateau and the possible sources and mechanisms for fertilization were investigated during ANTARES 3 (1995; Blain et al., 2001) and KEOPS 1 cruise, later referred to as KEOPS 1 (Jan.-Feb. 2005, late summer conditions; Blain et al., 2007, 2008). During KEOPS 2 the evolution of Chl-a data based on multi-satellite imagery of the study area revealed the presence of different Chl-a rich plumes (D'ovidio et al., 2014) (Fig.1a; e.g. Chl-a map from 11/11/2011). Stations were sampled in distinct zones covering these different bloom patterns (Fig.1a) (corresponding stations are reported in Fig1.b): (a) on the shallow plateau (station A3; see 1 in Fig.1a). Note that station A3 coincides with a site studied during the KEOPS 1 cruise, and that it was sampled twice over a 27-day period; (b) in a meander formed by a quasi-permanent retroflection of the Polar Front (PF) and topographically-steered by the eastern escarpment (Gallieni Spur) of the Kerguelen Plateau (mainly stations E, sampled as a quasi-lagrangian temporal series) (see 2 in Fig.1a); (c) along a North-South Transect (referred to as TNS stations; see 3, grey line in Fig.1a) and a West-East Transect (referred to as TEW stations; see 4, grey

192 line in Fig.1a), both crossing the PF; and (d) in the Polar Front Zone (PFZ) in
193 the vicinity (east) of the PF (station F-L; see 5 in Fig.1a). Furthermore we also
194 sampled a reference HNLC/non bloom/non Fe-fertilized station southwest of
195 the Plateau (station R-2; see 6 in Fig.1a). Station locations are given in Table
196 1.

197 Detailed descriptions of the complex physical structure of the area,
198 circulation, water masses and fronts are given in Park et al. (2014). Briefly,
199 the main hydrodynamic features observed during the cruise are the following
200 (see θ–S diagram, Fig.2a): (1) North of the PF, stations in the PFZ (TNS-1,
201 TEW-8 and F-L) present Antarctic Surface Waters (AASW; θ≃ 4°C and density
202 <27); θ–S characteristics between 150 to 400 m at station F-L (and to a
203 lesser extent at station TNS-1) reveal the presence of interleaving with waters
204 from northern (subantarctic) origin, centered between the 27.2 and 27.5
205 density curves, where Antarctic Intermediate Waters (AAIW) are usually
206 found. This contrasts with the situation at station TEW-8, where there is no
207 evidence of interleaving; (2) stations south of the PF exhibit subsurface
208 temperature minima characteristic of Winter Waters (WW); below the WW
209 three water masses can be identified, namely: the Upper (temperature
210 maximum) and Lower (salinity maximum) Circumpolar Deep Water (UCDW
211 and LCDW), and the Antarctic Bottom Water (AABW). Theses water masses
212 are present roughly in the following depth intervals: 700 m<UCDW< 1500 m;
213 1500 m <LCDW<2500 m; AABW>2500 m.

214 Based on the θ–S characteristics (Fig.2a, -2b) and surface
215 phytoplankton biomasses we can schematically group the stations as follows.
216 The R-2 HNLC reference station (white dot in Fig.1b) is characterized by a
217 very low biomass (with low iron contents; Quéroué et al., 2014). Stations
218 TEW-3 and TNS-8 (black dots) are characterized by a low to moderate
219 biomass and Fe contents. Stations A3 and E-4W (red dots; south of the PF) as
220 well as stations TNS-1, F-L and TEW-8 (blue dots; north of the PF) are

221 characterized by high biomass and iron contents. Stations in the core of the
222 PF meander (green dots; stations TNS-6, E-1, E-2, E-3, E-4E and E-5
223 considered as a temporal series) are characterized by moderate biomass and
224 iron contents.
225
226 **2.2. Sampling and analyses**
227 22 CTD casts (surface to 500-2000 m) were sampled for particulate
228 barium (Table 1) using a CTD-rosette equipped with 22 12L Niskin bottles.
229 Deep particulate Ba profiles (>1000 m) were not systematically obtained from
230 the same CTD cast, but from successive casts sampled closeby in time and
231 space and having similar θ-S data profiles. In the following, we use both the
232 station and CTD numbers to refer to stations.
233 4 to 7 L of seawater were filtered onto 47 mm polycarbonate
234 membranes (0.4 µm porosity) under slight overpressure supplied by filtered
235 air (0.4 µm). The filters were rinsed with Milli-Q grade water (<5 mL) to
236 remove sea salt, dried (50°C) and stored in Petri dishes for later analysis. In
237 the home-based laboratory we performed a total digestion of samples using a
238 tri-acid (0.5 mL HF/1.5 mL HCl/1 mL HNO_3; all Suprapur grade) mixture in
239 closed telfon beakers overnight at 90°C in a clean pressurized room. After
240 evaporation close to dryness samples were re-dissolved into around 13 mL of
241 HNO_3 2%. The solutions were analysed for Ba and other major and minor
242 elements by ICP-QMS (inductively coupled plasma-quadrupole mass
243 spectrometry; X Series 2 ThermoFisher) equipped with a collision cell
244 technology (CCT). To correct instrumental drift and matrix effects, internal
245 standards and matrix-matched calibrations were used. We analysed several
246 certified reference materials which consisted of dilute acid-digested rocks
247 (BHVO-1, JB-3 and JGb-1), natural riverine water (SLRS-5) and multi-element
248 artificial solutions for these external calibrations. Based on analyses of these
249 external standards, accuracy and reproducibility are better than ± 5%. For

more details on sample processing and analysis we refer to Cardinal et al. (2001). Among all elements analysed, particular interest went to Ba and Al. The presence of sea-salt was checked by analysing Na and the sea-salt particulate Ba contribution was found negligible. Average detection limits equal 0.6 nM for Al and 3 pM for Ba. Detection limits were calculated as three times the standard deviation on the blank measured on board and then normalized to an average dilution factor of 385, i.e., particles from around 5 L of Milli-Q water, dissolved in a final volume of 13 mL as for the samples. Biogenic barium (hereafter called excess-Ba or Ba_{xs}) was calculated as the difference between total particulate Ba and lithogenic Ba using Al as the lithogenic reference element (Dymond et al., 1992; Taylor and McLennan, 1985). At most sites and depths the biogenic Ba_{xs} represented >95% of total particulate Ba. Lithogenic Ba reached up to 20% of total particulate Ba at some depths in the upper 80-100 m, mainly at station R-2 and stations north of the Polar Front (i.e., TEW-8, F-L and TNS-1). The standard uncertainty (Ellison et al., 2000) on Ba_{xs} data ranges between 5 and 5.5%. Ba_{xs} and Al data are reported in Appendix A.

2.3. O_2 consumption and POC remineralization

The rate of oxygen consumption and particulate organic carbon remineralization rate in the mesopelagic layer (later referred to as MR) can be estimated using an algorithm relating mesopelagic Ba_{xs} contents and oxygen consumption based on earlier observations in the Southern Ocean (Shopova et al., 1995; Dehairs et al., 1997; 2008). The detailed calculations are described in Jacquet et al. (2008a, 2011a). Briefly, we use the following equations:

$$J_{O_2} = (Ba_{xs} - Ba_{residual})/17450 \qquad \text{(Eq.1)}$$

$$C_{respired} = Z \times J_{O_2} \times RR \qquad \text{(Eq.2)}$$

where J_{O2} is the O_2 consumption (µmol l^{-1} d^{-1}) and $C_{respired}$ is the Mineralization Rate of organic carbon (in mmol C m^{-2} d^{-1}; MR); Ba_{xs} is the depth-weighted average Ba_{xs} value (DWAv), i.e. the Ba_{xs} inventory divided by the depth layer considered Z, $Ba_{residual}$ is the residual Ba_{xs} signal (or Ba_{xs} background) at zero oxygen consumption and RR is the Redfield C/O_2 molar ratio (127/175; Broecker et al., 1985). DWAv Ba_{xs} values were calculated both for the 150 to 400 m (Plateau and deep stations) and the 150 to 800 m layers (deep stations only) (see details further below). The residual Ba_{xs} is considered as 'preformed' Ba_{xs}, left-over after partial dissolution and sedimentation of Ba_{xs} produced during a previous phytoplankton growth event. In $BaSO_4$ saturated waters, such as the ones filling the whole ACC water column (Monnin et al. 1999), this background Ba_{xs} value was considered to reach 180 to 200 pM which is rather characteristic for the deep ocean (>1000m) (see Dehairs et al., 1997; Jacquet et al., 2008a, 2011). In the present study we used a Ba_{xs} background of 180 pM.

We take the opportunity here to also compare O_2 consumption rates for the KEOPS 1 expedition (D. Lefèvre, unpublished data) with KEOPS 1 Ba_{xs} data published earlier (Jacquet et al., 2008a). No such O_2 consumption data are available for KEOPS 2. During KEOPS 1, dark community respiration (DCR) was estimated from changes in the dissolved oxygen concentration over 72 hours incubations. Discrete samples were collected at three depths in the mesopelagic zone from Niskin bottles into 125 cm^3 borosilicate glass bottles according to the WOCE procedure, and oxygen concentration was determined by Winkler titrations using a photometric endpoint detector (Williams and Jenkinson, 1982). By integrating DCR data in the water column we estimated the rate of oxygen consumption (later referred to as JO_2-W). We compared JO_2-W obtained from incubated oxygen samples with the rate of oxygen consumption based on KEOPS 1 mesopelagic Ba_{xs} contents (Eq.1; later referred to as JO_2-Ba). Dissolved oxygen was measured three times at

307 station A3 (same location as during KEOPS2) over a 19-day period (A3 CTD
308 #32, #74 and #119). Dissolved oxygen was also measured at station C11
309 located off-shelf in less productive HNLC waters (51.65°S, 78.00°E; not
310 shown in Fig.1) and was sampled two times over a 10-day period (C11
311 CTD#42 and #83). Fig.3 compares JO_2-W and JO_2-Ba for repeat stations A3
312 (#32, 74 and 119) and C11 (#42 and 83) (integration between 150-300 m).
313 JO_2-W range from 0.082 to 0.208 mmol m^{-2} d^{-1} at station A3 and from 0.292
314 to 0.528 mmol m^{-2} d^{-1} at station C11. Although JO_2-Ba rates (from 0.846 to
315 1.555 mmol m^{-2} d^{-1}) are slightly higher than JO_2-W, JO_2 rates are of the same
316 order of magnitude and present a same trend. We observe a significant
317 positive correlation between both JO_2 rates (R^2=0.90; $p<0.01$) with a slope of
318 0.64. The difference in oxygen consumption rates could be explained by the
319 integration time of both methods (few hours for the incubations vs. few days
320 to weeks for Ba_{xs}) and by the fact that KEOPS 1 occurred at the decline of the
321 bloom (late summer; low organic substrates), which would explain the lower
322 JO_2 rates as estimated by the incubation method.

323 Overall, these results highlight the need for further constraining spatial
324 and temporal variability of deep ocean oxygen utilisation via a combination of
325 direct rate measurements and the Ba_{xs} proxy. In the present work O_2
326 consumption and POC remineralisation was assessed from Ba_{xs} inventories
327 and Eqs.1 and 2. C remineralization rates are given in Table 1. Relative
328 standard uncertainties (Ellison et al., 2000) on C remineralization ranged
329 between 4 and 20%.

330

331 **3. RESULTS**

332 **3.1. Particulate biogenic Ba_{xs} profiles**

333 Ba_{xs} profiles in the upper 800 m are reported in Fig.4. The complete
334 whole water column data set is given in Appendix A. From previous studies we
335 know that Ba_{xs} in surface waters is distributed over different, mainly non-

336 barite biogenic phases (see Stroobants et al., 1991, Jacquet et al., 2007,
337 Cardinal et al., 2005, Sternberg et al., 2005). As such, these do not reflect
338 POC remineralization processes, in contrast to mesopelagic waters where Ba_{xs}
339 is mainly composed of barite (Dehairs et al., 1980) formed during prokaryotic
340 degradation of sinking POC (Martin et al., 1987; Sarmiento et al., 1993;
341 Buesseler et al., 2007b). For KEOPS 2 we observe that Ba_{xs} concentrations
342 generally increase below 150 m (i.e., they increase above the background
343 level set at 180 pM), but some sites have ocean surface Ba_{xs} contents
344 significantly larger than background (E-1,896 pM at 21 m; E4-E, 563 pM at 93
345 m). Such values are not unusual, and very high surface values have been
346 observed occasionally in earlier Southern Ocean studies. During KEOPS 1,
347 surface Ba_{xs} maxima at the three A3 repeats stations ranged from 1354 to
348 5930 pM at 50 m, likely associated with phytoplankton derived particles
349 (Jacquet et al., 2008a).

350 The following part focuses on the mesopelagic zone where most of the
351 remineralization of exported organic matter takes place. The Ba_{xs} profile for
352 station R-2 (CTD #17) displayed a characteristic mesopelagic Ba_{xs} maximum
353 reaching up to 834 pM at 304 m which is actually one of the highest values
354 observed for the whole study (Fig.4a). Ba_{xs} profiles for stations A3 above the
355 Kerguelen plateau (A3-1 CTD #4 and A3-2 CTD #107; Fig.4b) had lower
356 mesopelagic Ba_{xs} contents, with values ranging from about 80 to 350 pM. For
357 both A3 visits, Ba_{xs} values increased close to the seafloor reaching up to 1108
358 pM (A3-1, 474 m) and 1842 pM (A3-2, 513 m). In contrast, station E-4W
359 (located further north along the margin in deeper waters, but with similar θ–S
360 and Chl-a characteristics as station A3) displayed a large mesopelagic Ba_{xs}
361 maximum reaching up to 627 pM at 252 m (Fig.4c). Station TEW-3 (located
362 on the Kerguelen plateau, in waters with similar θ–S and Chl-a characteristics
363 as station TNS-8) had a profile similar to the one observed at station A3-2,
364 but compared to plateau sites A3-1 and A3-2 no increased Ba_{xs} contents were

observed in bottom water (Fig.4d). The other stations of the study area (Fig.4d-g) have Ba_{xs} profiles similar to the one at station E-4W, showing the characteristic Ba_{xs} maximum between 200 and 500 m. Note that for most of the stations, Ba_{xs} concentrations in waters below the mesopelagic maximum did not systematically decreased to reach the Ba_{xs} background level (180 pM; see above). In some cases Ba_{xs} contents significantly higher than residual Ba_{xs} were observed until below 1000 m (see Appendix A). This is particularly salient at stations TNS-6, E-1, E-2 and F-L where Ba_{xs} values below 1000 m reach 410 pM at 1886 m (TNS-6) and 436 pM at 1498 m (E-1). These cases of high deep Ba_{xs} contents clearly contrasted with the values observed at station E4-E (Fig.4h).

3.2. Depth-weighted average Ba_{xs} content of mesopelagic waters

Since the base of the mixed layer was generally shallower than ≤150 m, this depth is taken as the upper boundary of the mesopelagic domain. The depth-weighted average (DWAV) Ba_{xs} contents, calculated for the 150-400 m and 150-800 m depth intervals, are given in Table 1. For the profiles on the plateau (500 m water column) bottom waters with evidence of sediment resuspension were not taken into account when calculating DWAv Ba_{xs} values (≥ 400 m). Particle size spectra indicated that sediment resuspension occurred especially at stations A3 and TEW-3 (Jouandet et al., 2014; Lasbleiz et al., 2014; Van der Merve et al., 2015;). Thus, at site A3 (Fig.4b) DWAV Ba_{xs} was calculated for the layer between 150 and 354 m for A3-1 (CTD #4) and between 150 and 405 m for A3-2 (CTD#107). For station TEW-3 (CTD #38) DWAV Ba_{xs} was calculated for the water layer between 150 and 400 m (Fig.4d). For the deep sites, we considered both, the 150-400 m and the 150-800 m depth intervals, when calculating the DWAV Ba_{xs} contents. Depth weighted average Ba_{xs} values were translated into carbon remineralization

393 rates using equation (1) and (2) given above. These rates ranged from 2 to
394 91 mgC m^{-2} d^{-1} (Table 1).

395 DWAV Ba_{xs} values range from 199 to 572 pM (Table 1) and fit within
396 the range reported for Polar Front areas during previous studies (Cardinal et
397 al., 2001, 2005; Jacquet et al., 2005, 2008a, 2008b, 2011; Planchon et al.,
398 2013). For the KEOPS 2 cruise the main observed features are:

399 (a) Unexpectedly, the highest DWAV Ba_{xs} value of the whole study area
400 (572 pM; 150-400 m) was observed at the reference R-2 site. Bowie et al.
401 (2014), Quéroué et al. (2014) and van der Merve et al. (2015) reported for R-
402 2 local maxima in particulate and dissolved trace metals at 500 m and deeper,
403 reflecting lateral transport of lithogenic matter possibly originating from the
404 Leclaire Rise (a large seamount located west of R-2). Similarly, Lasbleiz et al.
405 (2014) observed a maximum of lithogenic silica (LSi) at 500 m, confirming
406 lithogenic inputs there. However, we note that the mesopelagic Ba_{xs}
407 maximum at R-2 occurs at shallower depths, around 300 m, and that there is
408 no evidence for elevated values at 500 m where the previous authors
409 reported higher trace element and silica concentrations. Also, as reported
410 above (see section 2.2 and Appendix A), the higher lithogenic Ba fractions at
411 R-2 (up to 20% of the total Ba) occur only in the upper 80 m. Moreover, we
412 do note that surface waters at R-2 experienced already some nitrate
413 consumption as compared to subsurface Winter Waters (Tmin waters).
414 Indeed, surface waters had 10% less nitrate than Winter Water (26 µM at 5 m
415 vs. 29 µM at 200 m) and the isotopic enrichment of this surface nitrate
416 confirmed an imprint of uptake (see Dehairs et al., 2014). Also, Lasbleiz et al.
417 (2014) report relatively low Si:C and Si:N ratios for surface ocean suspended
418 matter) pointing to the development of a diatom assemblage just prior the
419 sampling, consistent with the high dissolution rates of biogenic silica (BSi)
420 Closset et al. (2014) report for R-2 surface waters. It is therefore likely that
421 the mesopelagic Ba_{xs} content at R-2 indeed reflects remineralization of

organic material that was fuelled by an important past early spring production and export event. Similarly, F. Dehairs (unpublished results) observed the presence of significant numbers of barite microcrystals in mesopelagic waters at the KERFIX time series station (50°40'S, 68°25'E) located east of R-2 during late winter (Nov. 1993). Results would thus suggest the occurrence in this HNLC area of recurrent brief early spring diatom productive period pulses and subsequent export and remineralization activity in the underling layers. Chla satellite images (Giovani online Visualization and Analysis system, NASA GES DISC) corroborate that the R-2 and KERFIX area is occasionally subject to enhanced biomass during early spring;

(b) The two successive visits (27-day interval) at site A3 yielded relatively low DWAV Ba_{xs} values of 267 and 316 pM, and a quite similar value was observed for the shallow station TEW-3 (324 pM), located further north on the plateau, but north of the PF. Note that for comparison purposes, we recalculated the DWAV Ba_{xs} and MR values of KEOPS 1 by considering upper and lower mesopelagic layer boundaries of 150 and 400 m rather than 125 and 450 m, as in Jacquet et al. (2008a). Also, in the latter study the high Ba_{xs} contents observed near the seafloor were not excluded from the calculations, while they are here. These increased benthic boundary layer Ba_{xs} contents (observed also during KEOPS 2) are due to sediment resuspension which extended up to 70 m above the seafloor during KEOPS 1 (Blain et al., 2008; Venchiarutti et al., 2008; Armand et al., 2008). Because of these slightly different depth intervals over which Ba_{xs} values were integrated, the KEOPS 1 values discussed here will be slightly different from those reported in Jacquet et al. (2008a). At the other depths the lithogenic Ba contribution at A3 (KEOPS 2) was only minor;

(c) The time series stations in the Polar Front meander had DWAV Ba_{xs} contents ranging from 258 to 427 pM (150-400 m), so reaching values exceeding those on the plateau. For these time series stations values

451 decreased between day 0 (TNS-6) and 12 (E-3), and then increased again at
452 days 22 (E-4E) and 27 (E-5). Stations E-4W and TNS-8 above the plateau but
453 in deeper waters close to the Kerguelen margin, at the edge the high biomass
454 plume (Figure 1) had the highest DWAV Ba_{xs} values (468 and 473 pM,
455 respectively; 150-400 m), not considering the R-2 reference station. The
456 Polar Front F-L site, although located within the eastern part of the high
457 biomass plume had a smaller DWAV Ba_{xs} value of 345 pM (150-400 m) and
458 the close by station TEW-8 had the lowest DWAV Ba_{xs} value of the whole
459 study area (199 pM; 150-400 m).
460
461 **4. DISCUSSION**
462 **4.1. Mesopelagic Ba_{xs} and bacterial production**
463 Previous studies revealed that the shape of the column-integrated
464 bacterial production (BP) profile (i.e. the attenuation length scale) was
465 important in setting the Ba_{xs} signal in the mesopelagic zone (Dehairs et al.,
466 2008; Jacquet et al., 2008a, 2011a). Mesopelagic Ba_{xs} content is smaller
467 when most of the column integrated BP is restricted to the upper mixed layer
468 (indicating an efficient, close to complete remineralization within the surface),
469 compared to situations where a significant part of integrated BP was located
470 deeper in the water column (reflecting significant deep bacterial activity and
471 POC export). During KEOPS 2 the incorporation of ^{3}H-leucine was used to
472 estimate bacterial production. BP data are described in Christaki et al. (2014).
473 In Fig.5 we compare column-integrated BP at 150 m over 400 m (BP150/400)
474 and DWAV Ba_{xs} for the 150-400 m depth interval, next to the relation
475 obtained during KEOPS 1 (BP200/125 and 150-450 m DWAV Ba_{xs}; Jacquet et
476 al., 2008a; Christaki et al., 2008). Excluding stations A3, E-1, E-2 and E-3,
477 KEOPS 2 data presented a significant correlation (R^2=0.88; $p<0.01$) and a
478 similar trend to the one reported for KEOPS 1. A similar picture was obtained
479 when integrating DWAV Ba_{xs} and BP up to 800 m (not shown). The time series

480 "E" stations in the meander revealed a shift from stations E-1, E-2 and E-3 to
481 stations E-4E and E-5, i.e. towards the trend reported above. A shift was also
482 apparent at station A3 from KEOPS 2 (early spring) to KEOPS 1 (late
483 summer). It is thus possible that results reflect the occurrence of different
484 stage of bloom advancement. The large variability of Ba_{xs} and BP relationship
485 during KEOPS 2, especially at A3 site and in the meander, could reflect the
486 temporal evolution and patchiness of the establishment of mesopelagic
487 remineralization processes in this Polar Front area.
488
489 **4.2. Fate of exported organic C in the mesopelagic zone and deep**
490 **water column**
491 An important question relates to the fate of the exported POC: how
492 much of this POC is respired in the mesopelagic waters and how much
493 escapes remineralization and is exported to deeper layers where longer term
494 sequestration is likely (see e.g. Passow and Carlson, 2012; Robinson et al.,
495 2014; Schneider et al., 2008). To address these questions, we defined two
496 ratios: (1) the mesopelagic C remineralization efficiency (r-ratio in Table 2)
497 which is the ratio of mesopelagic C remineralization (MR, based on the DWAV
498 Ba_{xs} concentrations) over C export (EP) from the 150 m horizon (based on
499 ^{234}Th, see Planchon et al., this issue), and (2) the C transfer efficiency at 400
500 and 800 m (i.e., T400, T800 in Table 2) which is the fraction of C export (EP)
501 at 150 m passing through the 400 m (T400) or the 800 m (T800) horizons
502 (e.g., T400= EP400/EP150 = 1–(MR/EP150), with MR/EP150 = r-ratio; see
503 above). This approach is similar to the one developed by Buesseler and Boyd
504 (2009) stating that a conventional curve-fitting of particle flux data (i.e.,
505 power law or exponential) skews our interpretation of the mesopelagic
506 processes. They recommended the use of combined metrics to capture and
507 compare differences in flux attenuation. In the following, we compare MR
508 fluxes for the different KEOPS 2 areas (Reference site; Plateau sites; Polar

509 Front and Polar Front Meander) and discuss remineralization and transfer
510 efficiencies for those sites for which MR, primary production (PP) and/or EP
511 data (Table 2) were available. PP data were estimated from uptake
512 experiments including 24-hour incubations at different PAR levels over the
513 euphotic layer i.e., up to the 0,01% PAR level (Cavagna et al., 2014). EP data
514 were estimated from ^{234}Th activities and ^{234}Th /POC ratios and are discussed
515 in Planchon et al. (2014). The thorium method integrates POC export over a 1
516 month period (^{234}Th half live equals 24.1 days). We remind here that MR
517 fluxes as based on mesopelagic Ba_{xs} reflect past remineralization activity
518 integrated over several days to a few weeks (Dehairs et al., 1997; Cardinal
519 et al., 2005; Jacquet et al., 2007, 2008b). In order to compare EP with MR (r-
520 ratio and transfer efficiency) we consider EP fluxes from 150 m. Results are
521 compared with late summer KEOPS 1 results. For KEOPS 1, PP data are
522 detailed in Lefèvre et al. (2008) and Mosseri et al. (2008), EP data are
523 detailed in Savoye et al. (2008) and Ba_{xs} data are described in Jacquet et al.
524 (2008a).
525
526 **4.2.1. Reference station R-2**
527 Since station R-2 had the highest DWAV Ba_{xs} content it yielded the
528 highest MR flux of the whole study area (91 mgC m^{-2} d^{-1}; 150-800 m; Table
529 2). In contrast, both PP and EP fluxes at R-2 were very low (132 and 10 mgC
530 m^{-2} d^{-1}, respectively) and the calculated MR flux exceeded EP (Table 2). The
531 resulting export efficiency (EP/PP) was high, and T400 and T800 value (the
532 fraction of EP exported deeper than 400 m and 800 m, as defined above)
533 equal 0 (i.e., no export of POC beyond 400 and 800 m; note that >100%
534 values, i.e., MR>EP, were set to zero in Fig.7a and Table 2). The fact that MR
535 exceeds EP therefore implies a non-steady state condition at the R-2 site. As
536 reported above, R-2 probably experienced a brief early spring diatom
537 production pulse days to a few weeks before the start of the KEOPS 2 cruise,

538 followed by subsequent export and quite important remineralization activity in
539 the underling layers as depicted by MR data.
540
541 **4.2.2. Station A3 on the Plateau**
542 The MR fluxes on the plateau varied little between the two visits 27
543 days apart (Table 1) and as discussed below they were moreover similar to
544 summer values obtained during KEOPS 1 (see Jacquet et al., 2008a) when the
545 same A3 site was sampled 3 times over a 19-day period. While during KEOPS
546 2 (spring) MR fluxes at A3 ranged from 11 to 14 mgC m^{-2} d^{-1} (with a standard
547 uncertainty around 5%) they were slightly larger during KEOPS 1 (summer;
548 17 to 23 mgC m^{-2} d^{-1}) (Fig.5). We observed differences in the mesopelagic
549 POC remineralization efficiency between the two seasons (r-ratio, blue values
550 in Fig.6, Table 2). During KEOPS 1 r-ratios (MR/EP) remained low, ranging
551 from 7 to 9% of EP at A3, while during KEOPS 2 r-ratios were slightly higher
552 but decreased from 29% (A3-1; first visit) to 13%, 27 days later (A3-2;
553 second visit). This variation in r-ratio during KEOPS 2 is mostly due to an
554 increase of EP (from 47 to 85 mgC m^{-2} d^{-1}; Planchon et al., 2014) over the
555 same period while MR showed little change. Although at this early stage of the
556 season (spring) PP at A3-2 had already reached 2172 mgC m^{-2} d^{-1} (Cavagna
557 et al., 2014), EP remained relatively low (85 mgC m^{-2} d^{-1}). Here EP accounted
558 for only about 4% of PP (low export efficiency; see green data points in
559 Fig.5). This condition suggested that phytoplankton biomass was
560 accumulating in the surface waters without significant export yet, or that C
561 was channeled to higher trophic levels as suggested by Christaki et al.
562 (2014). Note that a negative relationship between primary productivity and
563 surface carbon export efficiency has already been reported from previous
564 studies in the Southern Ocean (Savoye et al., 2008; Morris et al., 2007;
565 Jacquet et al., 2011a; 2011b; Lam et al., 2007). Among possible explanations
566 for the occurrence of high productivity-low export efficiency regimes in high

567 latitude systems Maiti et al. (2013) mentioned differences in trophic structure,
568 grazing intensity, recycling efficiency, high bacterial activity, or increase in
569 DOC export, but the exact reason remain unclear. In contrast, during KEOPS
570 1 (summer), EP fluxes reached 250 mgC m^{-2} d^{-1} at 125 m (14-31% of PP)
571 while PP ranged from 865 to 1872 mgC m^{-2} d^{-1}, reflecting enhanced export
572 efficiency (Jacquet et al., 2008a; Savoye et al., 2008).

573 It is important to underline the fact that MR at station A3 was only
574 slightly higher in summer than in spring especially considering the large
575 differences in export efficiency between seasons. According to results from
576 sediment traps deployed over one year at the A3 site, Rembauville et al. (this
577 issue-b) reported that 60% of the annual POC export at the base of the mixed
578 layer occurred over a short periods of time representing <4% of the years
579 and was composed by small highly silicified, fast sinking, resting spores of
580 diatoms that bypass grazing pressure. According to these authors, the pulses
581 are linked to nutrient depletion dynamics inducing resting spore formation.
582 During the rest if the year, the flux was composed of small diatoms (empty
583 frustules) and small fecal pellets, with efficient C retention in the surface layer
584 or transfer to trophic levels. If we consider that export conditions during
585 KEOPS 2 are more similar to those prevailing most of the year, it is surprising
586 that during KEOPS 1 (that would reflect an export event toward the end of the
587 growth season) MR is not more important. This would indicate that fast
588 sinking- highly silicified- and pulsed material was directly transferred to the
589 bottom without major remineralization. Note for example that at the complex
590 R-2 reference station, a small export event (Laurenceau-Cornec et al.; this
591 issue) held heavily silicified diatoms (Lasbleiz et al.; 2014), and that the
592 material was efficiently remineralized in the upper mesopelagic layer as
593 witnessed by the high MR values we observe for that station. For the KEOPS 2
594 A3 site Laurenceau-Cornec et al. (2014) report that the sinking flux collected
595 in the upper layer using gel-filled sediment traps was composed by

phytodetrital aggregates that held slightly silicified diatoms (Lasbleiz et al., 2014). Even considering the shift from slightly- to highly-silicified material transfer between spring (KEOPS2) and summer (KEOPS 1), MR only slightly increases between both periods. Also, the mesozooplankton biomass at A3-2 was one of the highest of the KEOPS2 cruise, with a doubling from KEOPS 2 (early spring) to KEOPS 1 (late summer) (Carlotti et al., 2014). It is thus possible that at A3 the export event reported above, combined with a lasting grazing pressure would have induced this rather low and perduring mesopelagic remineralization. We also wonder whether the shallow water column at A3 combined with lateral advection above the plateau would play a role in triggering the mesopelagic POC remineralization activity and in setting its efficiency. For KEOPS 1, Venchiarutti et al. (2008) report that lateral advection over the plateau could significantly impact particle dynamics. During KEOPS 1, station B1 (CTD68) located on the plateau upstream from A3 according to the plateau circulation (Park et al., 2008) exhibited a very similar Ba_{xs} distribution as station A3: low mesopelagic Ba_{xs} and important bottom resuspension (not shown here; see Jacquet et al., 2008a). These strong similarities in Ba_{xs} profiles shape would indicate that next to the pulsed nature of the events, the dynamics on the shallow plateau play an important role in limiting the extend of mesopelagic POC remineralization processes.

In Fig.7a is shown for both KEOPS cruises the ratio of EP over PP (export efficiency) vs. the fraction of EP exported deeper than 400m (i.e. T400; defined above). Note that for station A3-1 (KEOPS 2), there are no PP data. The A3 site shows increasing EP/PP ratios from spring (KEOPS 2) to late summer (KEOPS 1), and so do the T400 values (A3-1: 70%; A3-2: 87%; KEOPS 1 A3 site: 92±1%). Station E-4W located in waters with similar θ-S and Chl-a characteristics as the A3 plateau site but has a deeper water column (1384 m has PP and EP fluxes of the same order of magnitude (Table 2). However, MR values (36 mgC m^{-2} d^{-1}; 150-400 m) are larger at E-4W,

625 resulting in a lower T400 value of around 33%, compared to 87% for A3-2
626 (Fig.7a). When integrating down to 800 m, T800 at E-4W equals 0 (i.e., no
627 export of POC beyond 800 m; Fig.7a and Table 2). Station F-L (in the vicinity
628 of the PF; 74.7°E) appears to function in a similar way as observed for E-4W
629 (71.4°E). PP at station F-L is relatively high (3380 mgC m^{-2} d^{-1}), while EP is
630 quite low (43 mgC m^{-2} d^{-1}), reflecting the fact that the biomass was not yet
631 exported from the surface waters or was transferred to higher trophic levels.
632 Since MR fluxes are slightly lower (21 mgC m^{-2} d^{-1}; 150-400 m) at F-L than at
633 E-4W, resulting T400 values are higher (52%) there.
634 Overall, during KEOPS 2 it appears that biomass at stations A3, E-4W
635 and F-L (sites of high productivity) was accumulating in surface waters (e.g.
636 transfer to higher trophic levels) and export did not start yet considering the
637 early stage of the season during KEOPS 2. Our observations allow us to
638 conclude the following:
639 (1) Both seasons (KEOPS 1 and KEOPS 2) showed a similar functioning of the
640 mesopelagic ecosystem at A3. The rather low and perduring MR fluxes under
641 high production and variable export regimes (high export efficiency during
642 KEOPS 1 and low export efficiency during KEOPS 2) indicated that here
643 mesopelagic remineralization does not represent a major resistance to organic
644 matter transfer to the sea-floor at A3. On average (considering both seasons,
645 but excluding A3-1) the C transfer efficiency into the deep (>400 m) as
646 assessed by PP, EP and MR fluxes comparisons reached 91±3% at A3;
647 (2) In contrast to A3, E-4W and F-L showed important mesopelagic
648 remineralization rates, reducing the efficiency of C transfer beyond 400 m to
649 33 and 52%, respectively, and to zero for both stations beyond 800 m.
650 Bottom depth, lateral advection, zooplankton grazing pressure and the pulsed
651 nature of the POC transfer at A3 were the particular conditions that could
652 drive the differences in C transfer efficiency between A3 and E4-W and F-L
653 and limit the extend of MR processes at A3.

654

655 **4.3. Stations in the meander**

656 Temporal short term changes for the stations TNS-6, E-1, E-2, E-3, E-
657 4E and E-5, located in the Polar front meander, will be discussed in this
658 section. Note that no PP or EP data exist for TNS-6. From Table 2 it appears
659 that PP almost doubled between E-1 and E-5 but this increase was not
660 paralleled by an increase of EP and MR, except for the 30% EP increase from
661 E-1 to E-3. In fact overall EP shows a decreasing trend with time, while MR
662 (150-400 m) stays rather constant, except for the decrease between E-1 and
663 E-3 (Table 2). As reported above such a mismatch may result from
664 differences in time scales characterizing the different processes that were
665 compared. The most likely explanation is that in this early stage of the growth
666 season, phytoplankton biomass was accumulating in the surface layer and
667 export was lagging behind.

668 The ratio of EP over PP vs. T400 and T800 showed a large variability in
669 transfer efficiency inside the meander (Fig.7b). PP and EP fluxes increased by
670 about 30% from E-1 to E-3, but a concomitant decrease of mesopelagic MR
671 yielded to an enhanced transfer efficiency, from 74 to 92%, through the 400
672 m boundary and from 52 to 73% through the 800 m boundary. This suggests
673 that significant remineralization should have occured at greater depths (even
674 > 1000 m) and it is also reflected by the presence of Ba_{xs} maxima below 1000
675 m (see Fig.4h and Appendix A). This was particularly salient when plotting
676 Ba_{xs} contents vs. depths over the 27-day observation period (Fig.8). The high
677 deep water Ba_{xs} values in Figure 8 were not taken into account when
678 integrating TNS-6 and E-1 profiles between 150 and 400 or even 150 and 800
679 m (Fig. 5e). Considering that the seafloor in the meander area is at about
680 2000 m depth, it seems unlikely that these high Ba_{xs} contents at depths
681 >1000 m were due to sediment resuspension. Also, particle spectra for these
682 sites do not reveal any bottom resuspension (Jouandet et al., 2014; Lasbleiz

683 et al., 2014; Vandermerve et al., 2015;). Therefore, the high deep (>1000 m)
684 Ba_{xs} contents at TNS-6 and E-1 most likely reflected the fact that here
685 significant remineralization of POC material did occur in the bathypelagic
686 domain and even down to the sea-floor. Note that suspended particles in the
687 depth range containing the deep Ba_{xs} maxima were dominated by the <2 µm
688 size fraction (Zhou et al., pers. comm.). When integrating the Ba_{xs} contents
689 from 150 m to the sea-floor at stations TNS-6 and E-1, MR fluxes increase to
690 156 and 184 mgC m^{-2} d^{-1} respectively. Such C fluxes were similar to the EP
691 values (maximum value of 130 mgC m^{-2} d^{-1} at E-3) and suggested that the
692 exported POC was entirely remineralized in the water column leaving no C for
693 transfer to the sediments.

694 Overall, the temporal pattern of mesopelagic remineralization
695 described above reflects two successive events of particle transfer: a first
696 transfer from a previous bloom (occurred before visiting TNS-6 and perduring
697 at E-1) and a second transfer from E-4E to E-5. The first transfer was evident
698 by the downward (up to the bottom) propagation of the mesopelagic Ba_{xs}
699 maximum signal, which mostly weakens at E-2. The second event was
700 reflected by the occurrence again of important mesopelagic Ba_{xs} build-up at E-
701 4E and E-5. Overall, our results indicated the large capacity of the Polar Front
702 Meander to transfer POC material to depth, but in contrast to station A3 on
703 the Plateau, this transfer was coupled to intense and near to complete POC
704 remineralization (as also observed at E-4W and F-L). Between-sites changes
705 in mesopelagic carbon remineralization due to unequal biomass productivity
706 and iron fertilization over the Kerguelen Plateau were thus relatively complex.
707 Furthermore, the situation in the Meander area seems to corroborate results
708 obtained in the iron-replete Subantarctic Zone east of the Tasman Plateau
709 (Australian sector of the Southern Ocean; SAZ-Sense cruise; Jacquet et al.,
710 2011a, 2011b), where the mesopelagic remineralization efficiency was
711 reported relatively high (on average 91%) and the deep (>600 m) carbon

712 transfer weak (<10%). Finally, the important Ba_{xs} contents reported between
713 1000 and 2000 m during the first stages of the meander time-series
714 strengthen recent results indicating for the Southern Ocean that 1000 m is
715 insufficient as an ocean-wide reference for carbon transfer and sequestration
716 potential (Robinson et al., 2014).
717
718 **5. Conclusion**
719 Based on spatially and temporally well resolved mesopelagic excess
720 particulate Ba inventories this work estimated mesopelagic POC
721 remineralization above the Kerguelen Plateau and inside a permanent
722 meander of the Polar Front to the east of Plateau, areas. The observed
723 variability of mesopelagic remineralization reflects differences in the fate of
724 the biomass that is exported to the deep ocean, between Plateau and Polar
725 Front. Results also reveal the patchiness of the season advancement and of
726 the establishment of remineralization processes between theses sites. Our
727 results indicate that the reference station R-2 experienced few days to weeks
728 before the start of the cruise an export event that was efficiently
729 remineralized in the upper mesopelagic layer. In terms of deep ocean carbon
730 transfer efficiency, our results highlight that above the plateau (A3 site)
731 mesopelagic remineralization is not a major barrier to organic matter transfer
732 to the sea-floor, with carbon transfer beyond 400 m reaching up to 87% of EP
733 during KEOPS 2, while in the Polar Front Meander remineralization of exported
734 organic carbon in the upper 400 m is more efficient than above the plateau.
735 In the Meander area remineralization may even balance export when including
736 its effect in the deeper waters (till 800 m and even deeper), thus resulting in
737 a close to zero carbon transfer to sediment. A similar condition is also
738 observed for sites at the margin of the plateau (E-4W) and the Polar front (F-
739 L).
740

Acknowledgements

We thank the officers and crew of R/V *Marion Dufresne* for their assistance during work at sea. We are indebted to chief scientist S. Blain and voyage leader B. Quéguiner for skillful leadership during the cruise and to the CTD team for managing rosette operation and CTD data. This research was supported by the French Agency of National Research grant (project KEOPS 2, #ANR-10-BLAN-0614), the Belgian Science Policy (BELSPO) project 'BIGSOUTH' (SD/CA/05A), Flanders Research Foundation (FWO Project G071512N), the European Union Seventh Framework Programme (Marie Curie CIG 'MuSiCC' under grant agreement n° 294146 to D.C.) and the Strategic Research Programme at Vrije Universiteit Brussel.

Figure captions

Figure 1: (a) Kerguelen Island area in the Southern Ocean with KEOPS 2 sampling zones and MODIS Chlorophyll concentrations (mg m^{-3}) (Chl-a map from 11/11/2011, courtesy F. d'Ovidio) superposed. 1 refers to station A3; 2 to stations E; 3 to the South-North Transect; 4 to the West-East Transect; 5 to station F-L and 6 to reference station R-2; (b) Corresponding stations location. Colors indicate stations with near similar θ–S and Chl-a characteristics.

Figure 2: (a) Potential temperature θ – salinity S plots and isopycnals for KEOPS 2 profiles, (b) Focus on the upper 200 m water column. AASW= Antarctic Surface Waters, AAIW= Antarctic Intermediate Waters, WW= Winter Waters, UCDW and LCDW= Upper and Lower Circumpolar Deep Water, AABW= Antarctic Bottom Water. Graph constructed using Ocean Data View (Schlitzer, 2002; Ocean Data View; http://www.awi-bremerhaven.de/GEO/ODV).

Figure 3: Rates of oxygen consumption (mmol m^{-2} d^{-1}) during KEOPS 1 as directly measured (JO_2-W) and from mesopelagic Ba_{xs} contents (JO_2-Ba). Rates are integrated between 150-300 m.

Figure 4: Particulate biogenic Ba_{xs} profiles (pM) in the upper 800 m (Fig.4a-g) and in the upper 2500 m (Fig.4h). Stations are identified by CTD cast numbers. BKG= Ba_{xs} background (180 pM).

Figure 5: Regression of the ratio of integrated bacterial production (BP) in the upper 150 m over integrated BP in the upper 400 m versus depth weighted average (DWAv) mesopelagic Ba_{xs} (pM; 150-400 m) during KEOPS 2. KEOPS 1 data (dots) are reported for comparison.

Figure 6: Schematic, comparing the fate of POC at station A3 during KEOPS 1 and KEOPS 2 cruises. PP= primary production, EP= export production at 150 m depth and MR= mesopelagic POC remineralization deduced from the Ba_{xs} maxima and integrated between 150-400 m; all fluxes in mgC m^{-2} d^{-1}. EP/PP (green values), MR/PP (red values) and MR/EP (r-ratio, blue values) ratios shown as %.

Figure 7: Y-axis: EP/PP = POC flux at 150 m (EP150) as a fraction of primary production (PP); X-axis: EPx/EP150 = POC flux at defined depths (EPx; here 400 and 800 m) as a fraction of POC flux at 150 m (EP150). The green cross (Fig.5a) is for station A3-1 (KEOPS-2). Since no PP data is available for that station, the EP/PP value has been arbitrarily set to 0. Isolines represent the modeled 1, 5, 10, 20 and 30% of PP export to depths >at 400 or 800 m, and represent export efficiency.

Figure 8: Temporal evolution of particulate biogenic Ba (Ba_{xs}; pM) in the upper 2000 m water column in the Polar Front meander. Graph constructed using Ocean Data View (Schlitzer, 2002; Ocean Data View; http://www.awi-bremerhaven.de/GEO/ODV).

Table captions

Table 1: Station locations, CTD cast number and bottom depth during KEOPS 2. Depth-weighted average values (DWAv) of mesopelagic Ba_{xs} (pM) and Ba_{xs} based mesopelagic POC remineralization (MR; mgC m^{-2} d^{-1}) integrated between 150-400 and 150-800 m depths. See text for further information on calculation.

Table 2: Comparison of mesopelagic POC remineralization (MR) with primary production (PP) and export production (EP). All fluxes in mg C m^{-2} d^{-1}. r-ratio is the ratio of MR over EP. EP/PP is the export efficiency. The C transfer efficiency at 400 and 800 m (T400, T800) is the fraction of C export (EP) at 150 m exiting through the 400 m (T400) or the 800 m (T800) horizons. See text for further information on calculation.

Appendix A: Excess particulate biogenic Ba (Ba_{xs}; pM) and particulate Al (nM) during KEOPS 2.

References

Armand, L.K., Crosta, X., Quéguiner, B., Mosseri, J., Garcia, N. : Diatoms preserved in surface sediments of the northeastern Kerguelen Plateau, Deep- Sea Res. Pt. II, 55, 677–692, 2008.

826 de Baar, H. J. W., Boyd, P. W., Coale, K. H., Landry, M.R., Tsud, A., Assmy,
827 P., Bakker, D.C.E, Bozec, Y., Barber, R.T., Brzezinski, M.A., Buesseler,
828 K.O., Boyé, M., Croot, P.L., Gervais, F., Gorbunov, Y., Harrison, P.J.,
829 Hiscock, W.T., Laan, P., Lancelot, C., Law, C.S., Levasseur, M., Marchetti,
830 A., Millero, F.J., Nishika, J., Nojiri, Y., van Oijen, T., Riebesell, U.,
831 Rijkenberg, M.J.A., Saito, H., Takeda, S., Timmermans, K.R., Veldhuis,
832 J.W., Waite, A.M., Wong, C.S.: Synthesis of iron fertilization experiments:
833 From the iron age in the age of enlightenment, J. Geophys. Res., 110,
834 C09S16, doi:10.1029/2004JC002601, 2005.
835 Blain, S., Tréguer, P., Belviso, S., Bucciarelli, E., Denis, M., Desabre, S., Fiala,
836 M., Martin Jézéquel, V., Le Fèvre, J., Mayzaud, P., Marty, J.- C., and
837 Razouls, S.: A biogeochemical study of the island mass effect in the
838 context of the iron hypothesis: Kerguelen Islands, Southern Ocean, Deep-
839 Sea Res. Pt. I, 48, 163-187, 2001.
840 Blain, S., Queguiner, B., Armand, L., Belviso, S., Bombled, B., Bopp, L.,
841 Bowie, A., Brunet, C., Brussaard, C., Carlotti, F., Christaki, U., Corbiere,
842 A., Durand, I., Ebersbach, F., Fuda, J. -L., Garcia, N., Gerringa, L.,
843 Griffiths, B., Guigue, C., Guillerm, C., Jacquet, S., Jeandel, C., Laan, P.,
844 Lefevre, D., Lo Monaco, C., Malits, A., Mosseri, J., Obernosterer, I., Park,
845 Y. -H., Picheral, M., Pondaven, P., Remenyi, T., Sandroni, V., Sarthou, G.,
846 Savoye, N., Scouarnec, L., Souhaut, M., Thuiller, D., Timmermans, K.,
847 Trull, T., Uitz, J., van Beek, P., Veldhuis, M., Vincent, D., Viollier, E., Vong,
848 L., and Wagener, T.: Effect of natural iron fertilization on carbon
849 sequestration in the Southern Ocean, Nature, 446, 1070-1074, 2007.
850 Blain, S., Quéguiner, B., and Trull, T.: The natural iron fertilization experiment
851 keops (kerguelen ocean and plateau compared study): An overview,
852 Deep-Sea Res. Pt. II, 55, 559–565, 2008.

853 Boyd, P. W., Bakker, D. C. E., Chandler, C.: A new database to explore the
854 findings from large-scale ocean iron enrichments experiments,
855 Oceanography, 25, 64–71, doi:10.5670/oceanog.2012.104, 2012.
856 Boyd, P. W., Law, C. S., Wong, C. S., Nojiri, Y., Tsuda, A., Levasseur, M.,
857 Takeda, S., Rivkin, R., Harrison, P. J., Strzepek, R., Gower, J., McKay, R.
858 M., Abraham, E., Arychuk, M., Barwell-Clarke, J., Crawford, W., Crawford,
859 D., Hale, M., Harada, K., Johnson, K., Kiyosawa, H., Kudo, I., Marchetti,
860 A., Miller, W., Needoba, J., Nishioka, J., Ogawa, H., Page, J., Robert, M.,
861 Saito, H., Sastri, A., Sherry, N., Soutar, T., Sutherland, N., Taira, Y.,
862 Whitney, F., Wong, S. K. E., and Yoshimura, T.: The decline and fate of an
863 iron-induced subarctic phytoplankton bloom, Nature, 428, 549–553, 2004.
864 Boyd, P. W., Watson, A. J., Law, C. S., Abraham, E. R., Trull, T., Murdoch, R.,
865 Bakker, D. C. E., Bowie, A. R., Buesseler, K. O., Chang, H., Charette, M.,
866 Croot, P., Downing, K., Frew, R., Gall, M., Hadfield, M., Hall, J., Harvey,
867 M., Jameson, G., LaRoche, J., Liddicoat, M., Ling, R., Maldonado, M. T.,
868 McKay, R. M., Nobber, S., Pickmere, S., Pridmore, R., Rintoul, S., Safi, K.,
869 Sutton, P., Strzepek, R., Tanneberger, K., Turner, S., Waite, A., and
870 Zeldis, J.: Phytoplankton bloom upon mesoscale iron fertilization of polar
871 Southern Ocean water, Nature, 407, 695–702, 2000.
872 Bowie, A. R., van der Merwe, P., Quéroué, F., Trull, T., Fourquez, M.,
873 Planchon, F., Sarthou, G., Chever, F., Townsend, A. T., Obernosterer, I.,
874 Sallée, J.-B., and Blain, S.: Iron budgets for three distinct biogeochemical
875 sites around the Kerguelen archipelago (Southern Ocean) during the
876 natural fertilisation experiment KEOPS-2, Biogeosciences Discuss., 11,
877 17861-17923, doi:10.5194/bgd-11-17861-2014, 2014.
878 Broecker, W. S., Takahashi, T., Takahashi, T.: Sources and flow patterns of
879 deep-ocean waters as deduced from potential temperature, salinity and
880 initial phosphate concentration, J. Geophys. Res., 90, 6925-6939, 1985.

881 Buesseler, K. O., Andrews, J.E., Pike, S.M., Charette, M.A.: The effect of iron
882 fertilization on carbon sequestration in the Southern Ocean, Science, 304,
883 414– 417, 2004.
884 Buesseler, K.O., Andrews, J.E., Pike, S.M., Charette, M.A., Goldson, L.E.,
885 Brzezinski, M.A., Lance, V.P.: Particle export during the Southern Ocean
886 Iron Experiment (SOFeX), Limnol. Oceanogr., 50 (1), 311– 327, 2005.
887 Buesseler, K.O., Antia, A.N., Chen, M., Fowler, S.W., Gardner, W.D.,
888 Gustaffson, Ö., Harada, K., Michaels, A.F., Rutgers van der Loeff, M.,
889 Sarin, M., Steinberg, D.K., Trull, T.: An assessment of the use of sediment
890 traps for estimating upper ocean particle fluxes. Journal of Marine
891 Research, 65(3): 345-416, 2007a.
892 Buesseler, K.O., Lamborg, C.H., Boyd, P.W., Lam, P.J., Trull, T.W., Bidigare,
893 R.R., Bishop, J. K. B., K.L., Casciotti, Dehairs, F. , Elskens, M. , Honda,
894 M. , Karl, D. M., Siegel, D. A., Silver, M. W., Steinberg, D.K. , Valdes, J.,
895 Van Mooy, B. , Wilson, S. : Revisiting carbon flux through the ocean's
896 twilight zone, Science, 316, 567–569, 2007b.
897 Buesseler, K.O., and Boyd, P.W.: Shedding light on processes that control
898 particle export and flux attenuation in the twilight zone. Limnol.
899 Oceanogr., 54 (4), 1210-1232, 2009.
900 Cardinal, D., Dehairs, F., Cattaldo, T., and André, L.: Constraints on export
901 and advection in the Subantarctic and Polar Front Zones, south of
902 Australia from the geochemistry of suspended particles, J. Geophys. Res.-
903 Oceans, 106, 31637-31656, doi : 10,1029/2000JC000251, 2001
904 Cardinal, D., Savoye, N., Trull., T.W., André, L., Kopczynska, E., Dehairs, F.,
905 2005. Particulate Ba distributions and fluxes suggest latitudinal variations
906 of carbon mineralization in the Southern ocean, Deep-Sea Res. Pt. I, 52,
907 355-370, 2005.
908 Carlotti, F., Jouandet, M.-P., Nowaczyk, A., Harmelin-Vivien, M., Lefèvre, D.,
909 Guillou, G., Zhu, Y., Zhou, M. : Mesozooplankton structure and functioning

910 during the onset of the Kerguelen Bloom during Keops2 survey, this issue,
911 in prep.
912 Cavagna, A. J., Fripiat, F., Elskens, M., Dehairs, F., Mangion, P.,
913 Chirurgien, L., Closset, I., Lasbleiz, M., Flores–Leiva, L., Cardinal, D.,
914 Leblanc, K., Fernandez, C., Lefèvre, D., Oriol, L., Blain, S., and
915 Quéguiner, B.: Biological productivity regime and associated N cycling in
916 the vicinity of Kerguelen Island area, Southern Ocean, Biogeosciences
917 Discuss., 11, 18073-18104, doi:10.5194/bgd-11-18073-2014, 2014.
918 Closset, I., Lasbleiz, M., Leblanc, K., Quéguiner, B., Cavagna, A.-J., Elskens,
919 M., Navez, J., and Cardinal, D.: Seasonal evo- lution of net and
920 regenerated silica production around a natu- ral Fe-fertilized area in the
921 Southern Ocean estimated from Si isotopic approaches, Biogeosciences,
922 11, 5827-5846, doi: 10.5194/bg-11-5827-2014, 2014.
923 Christaki, U., Obernosterer, I., VanWambeke, F., Veldhuis, M., Garcia, N., and
924 Catala, P.: Microbial food web structure in a naturally iron fertilized area in
925 the southern ocean (Kerguelen plateau), Deep-Sea Res. Pt. II, 55, 706–
926 719, 2008.
927 Christaki, U., Lefèvre, D., Geoges, C., Colombet, J., catala, P., Courties, C.,
928 Sime-Ngando, T., Blain, S., and Obernosterer, I.: Microbial food web
929 dynamics during spring phytoplankton blooms in the naturally iron-
930 fertilized Kerguelen area (Southern Ocean), Biogeosciences, 11, 6739-
931 3753, doi:10.5194/bg-11-6739-2014, 2014.
932 Dehairs, F., Chesselet, R., Jedwab, J.: Discrete suspended particles of barite
933 and the barium cycle in the open ocean, Earth Planet. Sc. Lett., 49, 40-42,
934 1980.
935 Dehairs, F., Baeyens, W., Goeyens, L.: Accumulation of suspended barite at
936 mesopelagic depths and export production in the Southern Ocean, Science**,**
937 258, 1332–1335, 1992.
938 Dehairs, F., Shopova, D., Ober, S., Veth, C., Goeyens, L.: Particulate barium

939 stocks and oxygen consumption in the Southern Ocean mesopelagic water
940 column during spring and early summer: Relationship with export
941 production, Deep-Sea Res. Pt II, 44, 497-516, 1997.
942 Dehairs, F., Jacquet, S.H.M., Savoye, N., van Mooy, B., Buesseler, K., Bishop,
943 J., Lamborg, C., Elskens, M., Baeyens, W., Casciotti K., Monnin , C.:
944 Barium in twilight zone suspended matter as proxy for organic carbon
945 mineralization: results for the North Pacific, Deep-Sea Res. Pt. II, 55,
946 1673-1683, 2008.
947 Dehairs, F., Fripiat, F., Cavagna, A.-J., Trull, T. W., Fernandez, C., Davies, D.,
948 Roukaerts, A., Fonseca Batista, D., Planchon, F., and Elskens, M.: Nitrogen
949 cycling in the Southern Ocean Kerguelen Plateau area: evidence for
950 significant surface nitrification from nitrate isotopic compositions,
951 Biogeosciences Discuss., 11, 13905-13955, doi:10.5194/bgd-11-13905-
952 2014, 2014.
953 D'ovidio, F., Della Penna, A., Trull, T.W., Nencioli, F., Pujol, I., Rio, M.H., Park,
954 Y.H., Cotté, C., Zhou, M., Blain, S.: The biogeochemical structuring role of
955 horizontal stirring: Lagrangian perspectives on iron delivery downstream of
956 the Kerguelen plateau, in prep., this issue.
957 Dymond, J.R., Suess, E., Lyle, M.: Barium in deep-sea sediment: a
958 geochemical proxy for paleoproductivity, Paleoceanography, 7, 163–181,
959 1992.
960 Ellison, Eurachem/CITAC Guide CG4, Quantifying Uncertainty in Analytical
961 Measurement. Eds. S.L.R. Ellison, M. Rosslein and A. Williams. Second
962 edition ISBN 0948926 15 5, Pp 120, 2000.
963 François, R., Honjo, S., Krishfield, R., and Manganini, S.: Factors controlling
964 the flux of organic carbon to the bathypelagic zone of the ocean, Global
965 Biogeochem. Cy., 16(4), 1087 doi:10.1029/2001GB001722, 2002.

966 Gervais, F., Riebesell, U., Gorbunov, M. Y.: Changes in primary productivity
967 and chlorophyll a in response to iron fertilization in the southern Polar
968 Frontal Zone, Limnol. Oceanogr., 47, 1324–1335, 2002.
969 Henson, S. A., et al. (2011), A reduced estimate of the strength of the
970 ocean's biological carbon pump, Geophys. Res. Lett., 38(4), L04606.
971 Hoffmann, L., Peeken, I., Lochte, K., Assmy, P., Veldhuis, M.: Different
972 reactions of Southern Ocean phytoplankton size classes to iron
973 fertilization, Limnol. Oceanogr, 51, 1217–1229, 2006.
974 Jacquet, S.H.M., Dehairs, F., Cardinal, D., Navez, J., Delille, B.: Barium
975 distribution across the Southern Ocean Frontal system in the Crozet-
976 Kerguelen Basin, Mar. Chem., 95(3-4), 149-162, 2005.
977 Jacquet, S.H.M., Dehairs, F., Elskens, M., Savoye, N., Cardinal, D.: Barium
978 cycling along WOCE SR3 line in the Southern Ocean, Mar. Chem., 106, 33-
979 45, 2007.
980 Jacquet, S.H.M., Dehairs, F., Savoye, N., Obernosterer, I., Christaki, U.,
981 Monnin, C., Cardinal, D.: Mesopelagic organic carbon mineralization in the
982 Kerguelen Plateau region tracked by biogenic particulate Ba, Deep-Sea
983 Res. Pt. II, 55 (5-7), 868-879, 2008a.
984 Jacquet, S.H.M., Savoye, N Dehairs, F., Strass, V., Cardinal, D.: Mesopelagic
985 carbon mineralization during the European Iron Fertilization Experiment
986 (EIFEX), Glob. Biogeochem. Cy., 22, GB1023,
987 doi:10.1029/2006GB002902, 2008b.
988 Jacquet, S.H.M., Dehairs, F., Becquevort, S., Dumont, I., Cavagna, A.,
989 Cardinal, D.: Twilight zone organic carbon remineralization in the PFZ and
990 SAZ south of Tasmania (Southern Ocean), Deep-Sea Res. Pt. II, 58 (22-
991 21), 2222-2234 doi:10.1016/j.dsr2.2011.05.029, 2011a.
992 Jacquet, S.H.M., Lam, P., Trull ,T., Dehairs, F.: Carbon export production in
993 the Polar front zone and Subantarctic Zone south of Tasmania, Deep-Sea

994 Res. Pt. II, 58 (21-22), 2277-2292 doi:10.1016/j.dsr2.2011.05.035,
995 2011b.
996 Jouandet, M.P., and others: Particles distribution in contrasted area of the iron
997 fertilized region around Kerguenlen Islans, in prep., this issue.
998 Lam, P. J., and Bishop, J. K. B.: High biomass, low export regimes in the
999 Southern Ocean, Deep-Sea Research II, 54, 601-638, 2007.
1000 Lampitt, R. S., Achterberg, E.P., Anderson, T.R., Hughes, J.A., Iglesisas-
1001 Rodriguez, M.D., Kelly-Gerreyn, B.A., Lucas, M., Popova, E.E., Sanders,
1002 R., Shepherd, J.G., Smythe-Wright, D., Yool, A. : Ocean fertilization: A
1003 potential means of geoengineering?, Philos. Trans. R. Soc. A, 366, 3919–
1004 3945, doi:10.1098/rsta.2008.0139, 2008.
1005 Lampitt, R. S., Antia, A.N.: Particle flux in deep seas: regional characteristics
1006 and temporal variability, Deep-Sea Res. Pt I, 44, 1377-1403, 1997.
1007 Lasbleiz, M., Leblanc, K., Blain, S., Ras, J., Cornet-Barthaux, V., Hélias
1008 Nunige, S., and Quéguiner, B.: Pigments, elemental composition (C, N, P,
1009 and Si), and stoichiometry of particulate matter in the naturally iron
1010 fertilized region of Kerguelen in the Southern Ocean, Biogeosciences, 11,
1011 5931–5955, doi::10.5194/bg-11- 5931-2014, 2014.
1012 Laurenceau-Cornec, E. C., Trull, T. W., Davies, D. M., Bray, S. G., Doran, J.,
1013 Planchon, F., Carlotti, F., Jouandet, M.-P., Cavagna, A.-J., Waite, A. M.,
1014 and Blain, S.: The relative importance of phytoplankton aggregates and
1015 zooplankton fecal pellets to carbon export: insights from free-drifting
1016 sediment trap deployments in naturally iron-fertilised waters near the
1017 Kerguelen plateau, Biogeosciences Discuss., 11, 13623-13673,
1018 doi:10.5194/bgd-11-13623-2014, 2014.
1019 Laws, E. A., et al. (2000), Temperature effects on export production the
1020 ocean, Global Biogeochem. Cycles, 14(4), 1231–1246.
1021 Lefèvre, D., Guigue, C., Obernosterer, I.: The metabolic balance at two
1022 contrasting sites in the Southern Ocean: the iron-fertilized Kerguelen area

and HNLC waters, Deep-Sea Res. Pt. II, 55, 766–776, doi:10.1016/j.dsr2.2007.12.006, 2008.

Le Moigne, F. A. C., Moore, C. M., Sanders, R. J., Villa-Alfageme, M., Steigenberger, S., and Achterberg, E. P.: Sequestration efficiency in the iron-limited North Atlantic: Implications for iron supply mode to fertilized blooms, Geophys. Res. Lett., 41, doi:10.1002/2014GL060308, 2014.

Longhurst, A.R., Bedo, A.W., Harrison, W.G., Head, E.J.H., Sameoto, D.D. : Vertical flux of respiratory carbon by oceanic diel migrant biota, Deep-Sea Res Pt, 37 (4), 685–694, 1990.

Maiti, K., Charette, M., Buesseler, K., and Kahru, M.: An inverse relationship between production and export efficiency in the Southern Ocean, Geophys. Res. Lett., 40, 2013.

Martin, J.H., Knauer, G.A., Karl, D.M., Broenkow, W.W.: VERTEX: carbon cycling in the NE Pacific, Deep-Sea Res., 34, 267–285, 1987.

Monnin, C., Jeandel, C., Cattaldo, T., Dehairs, F.: The marine barite saturation state of the world's oceans, Mar. Chem., 65(3-4), 253-261, 1999.

Morris, P.J, and Charette, M.A.: A synthesis of upper oceancarbon and dissolved iron budgets for Southern Ocean natural iron fertilization studies (2013), Deep-Sea Res., 90, 147-157, 2013.

Passow, U., Carlson, C. A. : The biological pump in a high CO2 world, Mar. Ecol. Prog. Ser., 470, 249–271, doi:10.3354/meps09985, 2012.

Porris, P.J., Sanders, R., Turnewithsch, R., Thomalla, S., 234^{Th}-derived particulate organic carbon export from an island-induced phytoplankton blomm in the Southern Ocean,Deep-Sea Res. Pt.II, 24, 2208-2232, 2007

Mosseri, J., Quéguiner, B., Armand, L. K., and Cornet-Barthaux, V.: Impact of iron on silicon utilization by diatoms in the Southern Ocean: a case study of Si/ N cycle decoupling in a naturally iron-enriched area, Deep-Sea Res. Pt. II, 55, 801-819, doi :10,1016/j.dsr2,2007,12,003, 2008.

1051 Park, Y. H., Durand, I., Kestenare, E., Rougier, G., Zhou, M., d'Ovidio, F.,
1052 Cotté, C., and Lee J. H.: Polar front around the Kerguelen islands: An up-
1053 to-date determination and associated circulation of surface/subsurface
1054 water. J. Geophys. Res. Oceans, 119, i10.1002/2014JC010061, 2014.
1055 Park, Y.-H., Roquet, F., Durand, I., and Fuda, J.-L.: Large-scale circulation
1056 over and around the Northern Kerguelen Plateau, Deep-Sea Res. Pt. II, 55,
1057 566–581, doi:10.1016/j.dsr2.2007.12.030, 2008.
1058 Planchon, F., Cavagna A.J., Cardinal, D., André, L., Dehairs, F. Late summer
1059 particulate organic carbon export and twilight zone remineralisation in the
1060 Atlantic sector of the Southern Ocean, Biogeosciences, 10, 803–820,
1061 doi:10.5194/bg-10-803-2013, 2013.
1062 Planchon, F., Ballas, D., Cavagna A. J., Van Der Merwe, P., Bowie, A., Trull,
1063 T., Laurenceau, E., Davis, D., and Dehairs, F.: Carbon export in the
1064 naturally iron fertilized Kerguelen area of the Southern Ocean using
1065 234Th-based approach, in prep., 2014.
1066 Pollard, R. T., Salter, I., Sanders, R. J., Lucas, M. I., Moore, C. M., Mills, R. A.,
1067 Statham, P. J., Allen, J. T., Baker, A. R., Bakker, D. C. E., Charette, M. A.,
1068 Fielding, S., Fones, G. R., French, M., Hickman, A. E., Holland, R. J.,
1069 Hughes, J. A., Jickells, T. D., Lampitt, R. S., Morris, P. J., Nedelec, F. H.,
1070 Nielsdottir, M., Planquette, H., Popova, E. E., Poulton, A. J., Read, J. F.,
1071 Seeyave, S., Smith, T., Stinchcombe, M., Taylor, S., Thomalla, S.,
1072 Venables, H. J., Williamson, R., and Zubkov, M. V.: Southern Ocean deep-
1073 water carbon export enhanced by natural iron fertilization, Nature, 457,
1074 577-U581, Doi 10.1038/Nature07716, 2009.
1075 Quéroué, F., Sarthou, G., Planquette, H. F., Bucciarelli, E., Chever, F.,
1076 van der Merwe, P., Lannuzel, D., Townsend, A. T., Cheize, M., Blain, S.,
1077 d'Ovidio, F., and Bowie, A. R.: High variability of dissolved iron
1078 concentrations in the vicinity of Kerguelen Island (Southern Ocean),

1079 Biogeosciences Discuss., 12, 231-270, doi:10.5194/bgd-12-231-2015,
1080 2015.
1081 Rembauville, M., Blain, S., Armand, L., Quéguiner, B., and Salter, I.: Export
1082 fluxes in a naturally fertilized area of the Southern Ocean, the Kerguelen
1083 Plateau: ecological vectors of carbon and biogenic silica to depth (Part 2),
1084 Biogeosciences Discuss., 11, 17089-17150, doi:10.5194/bgd-11-17089-
1085 2014, 2014.
1086 Robinson, J., Popova, E. E., Yool, A., Srokosz, M. A., Lampitt, R. S., and
1087 Blundell, J. R.: How deep is deep enough? Ocean iron fertilization and
1088 carbon sequestration in the Southern Ocean, Geophys. Res. Lett., 41,
1089 2489-2495, 2014.
1090 Salter, I., Lampitt, R.S., Sanders, R., Poulton, A., Kemp, A.E.S., Boorman, B.,
1091 Saw, K., Pearce, R.: Estimating carbon, silica and diatom export from a
1092 naturally fertilised phytoplankton bloom in the Southern Ocean using
1093 PELAGRA: a novel drifting sediment trap, Deep-Sea Res. Pt. II, 54, 2233–
1094 2259, 2007.
1095 Sarmiento, J.L., Slater, R.D., Fasham, M.J.R., Ducklow, H.W., Toggweiler,
1096 J.R.: A seasonal three-dimensional ecosystem model of nitrogen cycling in
1097 the North Atlantic photic zone, Global Biogeochem. Cy., 7, 417–450, 1993.
1098 Savoye, N., Trull, T., Jacquet, S.H.M., Navez, J., Dehairs, F.: ^{234}Th-derived
1099 export fluxes during a natural iron fertilization experiment (KEOPS), Deep-
1100 Sea Res. Pt. II, 55 (5-7), 841-855, 2008.
1101 Schlitzer, R., Ocean Data View, http://www.awi-bremerhaven.de/GEO/ODV,
1102 2002.
1103 Schneider, B., Bopp, L., Gehlen, M.: Assessing the sensitivity of modeled
1104 airsea CO2 exchange to the remineralization depth of particulate organic
1105 and inorganic carbon, Global Biogeochem. Cy., 22, GB3021, doi:10.1029/
1106 2007GB003100, 2008.

1107 Shopova, D., Dehairs, F., Baeyens, W.: A simple model of biogeochemical
1108 element distribution in the oceanic water column, J. Mar. Sy., 6, 331–344,
1109 1995.

1110 Smetacek, V., Klass, C., Strass, V.H., Assmy, P., %ontresor, M., Cisewki, B.,
1111 Savoye, N., Webb, A., d'Ovidio, F., Arrieta, J.M., Bathmann, U., Bellerby,
1112 R., Mine Berg, G., Croot, P., Gonzalez, S., Jenjes, J., Herndl, G.J.,
1113 Hoffmann, L.J., Leach, H., Losh, M., Mills, M.M., Neill, C., Peeken, I.,
1114 Rottgers, R., Sachs, O., Sauter, E., Schmidt, M.M., Schwarz, J.,
1115 Terbruggen, A., Wolf-Gladrow, D. : Deep carbon export from a Southern
1116 Ocean iron-fertilized diatom bloom, Nature, 487, 313–319,
1117 doi:10.1038/nature11229, 2012.

1118 Sternberg, E., Jeandel, C., Miquel, J.-C., Gasser, B., Souhaut, M., Arraes-
1119 Mescoff, R., Francois R. : Particulate barium fluxes and export production
1120 in the northwestern Mediterranean. Mar. Chem. 105, 281–295, 2007.

1121 Sternberg, E., Jeandel, C., Robin, E., Souhaut, M.: Seasonal cycle of
1122 suspended barite in the Mediterranean Sea, Geochimica et Cosmochimica
1123 Acta, 72, 4020-4034, 2008a.

1124 Sternberg, E., Tang, D., Ho, T_Y., Jeandel, C., Morel, M.M..: Barium uptake
1125 and adsorption in diatoms, Geochimica et Cosmochimica Acta, 69, 11,
1126 2745-2752, 2008b.

1127 Strass, V., Cisewski, B., Gonzales, S., Leach, H., Loquay, K.-D., Prandke, H.,
1128 Rohr, H., Thomas, M.: The physical setting of the European Iron
1129 Fertilization Experiment 'EIFEX' in the Southern Ocean, Reports on Polar
1130 and Marine Research, 500, 15–49, 2005.

1131 Stroobants, N., Dehairs, F., Goeyens, L., Vanderheijden, N., Van Grieken, R.:
1132 Barite formation in the Southern Ocean water column, Mar. Chem., 35,
1133 411-422, 1991.

1134 Taylor, S.R., McLennan, S.M.: The continental crust: its composition and
1135 evolution, Blackwell Scientific Publications, 312pp, 1985.

1136 van der Merwe, P., Bowie, A. R., Quéroué, F., Armand, L., Blain, S.,
1137 Chever, F., Davies, D., Dehairs, F., Planchon, F., Sarthou, G.,
1138 Townsend, A. T., and Trull, T.: Sourcing the iron in the naturally-fertilised
1139 bloom around the Kerguelen Plateau: particulate trace metal dynamics,
1140 Biogeosciences Discuss., 11, 13389-13432, doi:10.5194/bgd-11-13389-
1141 2014, 2014.

1142 Venchiarutti, C., Jeandel, C., Roy-Barman, M.: Particle dynamics study in the
1143 wake of Kerguelen Island using thorium isotopes, Deep-Sea Res. Pt. I, 55,
1144 1343–1363, 2008.

1145 Williams, P.J., Jenkinson, N.W. : A transportable microprocessor-controlled
1146 precise Winkler titration suitable for field station and shipboard use.
1147 Limnol. Oceanogr. 27, 576-585, 1982.

1148 Zhou, M., Zhu, Y., Dorland, R.D., Measures, C.I.: Dynamics of the current
1149 system in the southern Drake Passage, Deep-Sea Res. Pt I, 57, 1039–
1150 1048, 2010.

1151 Zhou, M., Zhu, Y., Measures, C.I., Hatta, M., Charette, M.A., Gille, S.T.,
1152 Frants, M., Jiang, M., Mitchell, B.G.: Winter mesoscale circulation on the
1153 shelf slope region of the southern Drake Passage, Deep-Sea Res. Pt II, 90,
1154 4–14, 2013.

1155 Zhou, M., and others: Estimates of particle settling and scavenging using
1156 LISST-LOPC in Kergueln Plateau regions during the 2011 austral spring
1157 KEOPS II cruise, in prep., this issue.

1158

1159

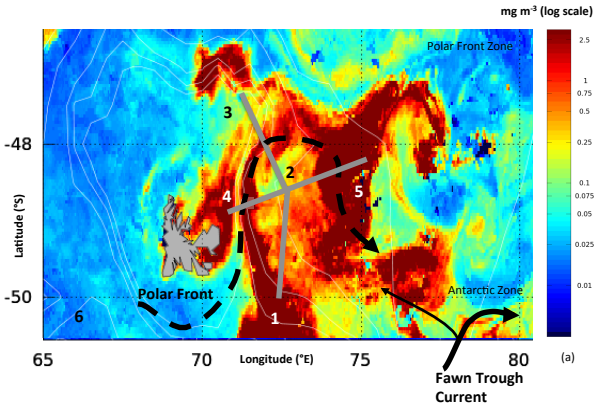
mg m-3 (log scale)
2.5
1
0.75
0.5
0.25
0.1
0.075
0.05
0.025
0.01
Polar Front Zone
Antarctic Zone
Polar Front
Fawn Trough Current
1
2
3
4
5
6
-48
-50
Latitude (°S)
65
70
75
80
Longitude (°E)
(a)

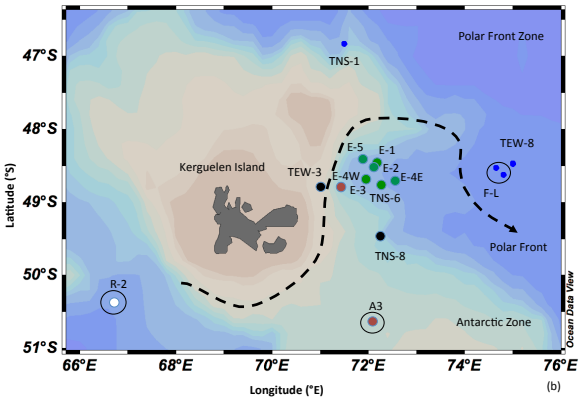
Polar Front Zone
TNS-1
47°S
48°S
49°S
50°S
51°S
Latitude (°S)
Kerguelen Island
TEW-3
E-5
E-1
E-2
E-4E
E-4W
E-3
TNS-6
TEW-8
F-L
Polar Front
TNS-8
R-2
A3
Antarctic Zone
66°E
68°E
70°E
72°E
74°E
76°E
Longitude (°E)
Ocean Data View
(b)

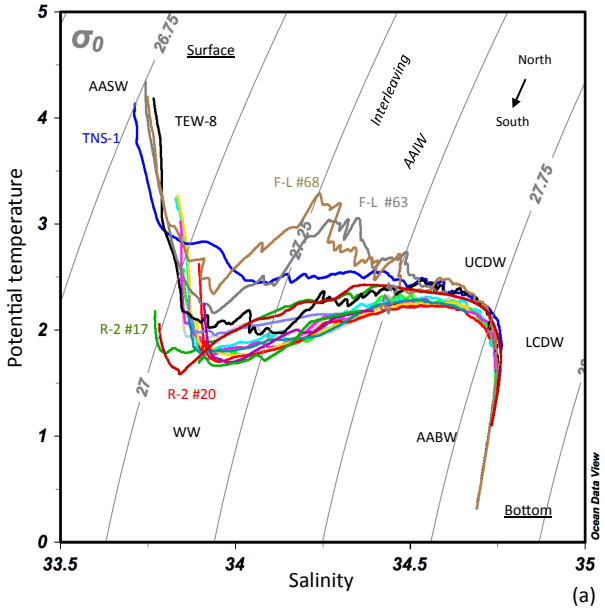
σ0
Surface
AASW
TEW-8
TNS-1
Interleaving
AAIW
North
South
F-L #68
F-L #63
UCDW
LCDW
R-2 #17
R-2 #20
WW
AABW
Bottom
26.75
27.75
27
Potential temperature
Salinity
Ocean Data View
(a)

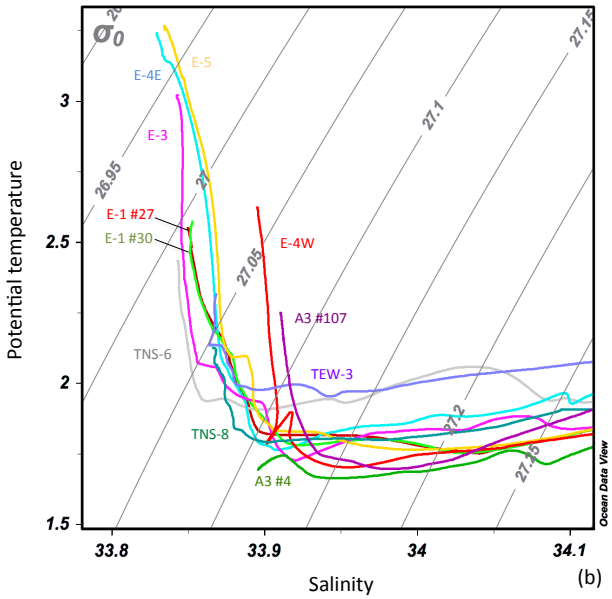
σ0
E-5
E-4E
E-3
E-1 #27
E-1 #30
E-4W
A3 #107
TNS-6
TEW-3
TNS-8
A3 #4
26.95
27
27.05
27.1
27.2
27.15
Potential temperature
Salinity
Ocean Data View
(b)

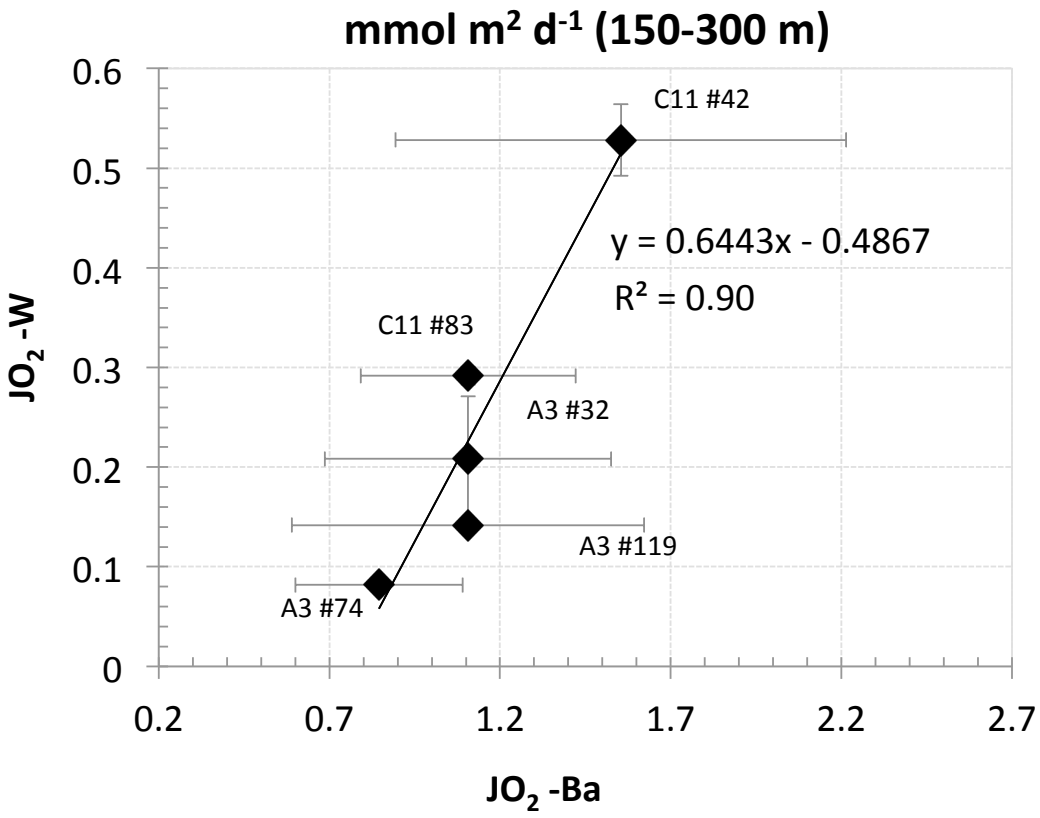
mmol m² d⁻¹ (150-300 m)
0.6
0.5
0.4
0.3
0.2
0.1
0
0.2
0.7
1.2
1.7
2.2
2.7
JO2 -W
JO2 -Ba
C11 #42
y = 0.6443x - 0.4867
R² = 0.90
C11 #83
A3 #32
A3 #119
A3 #74

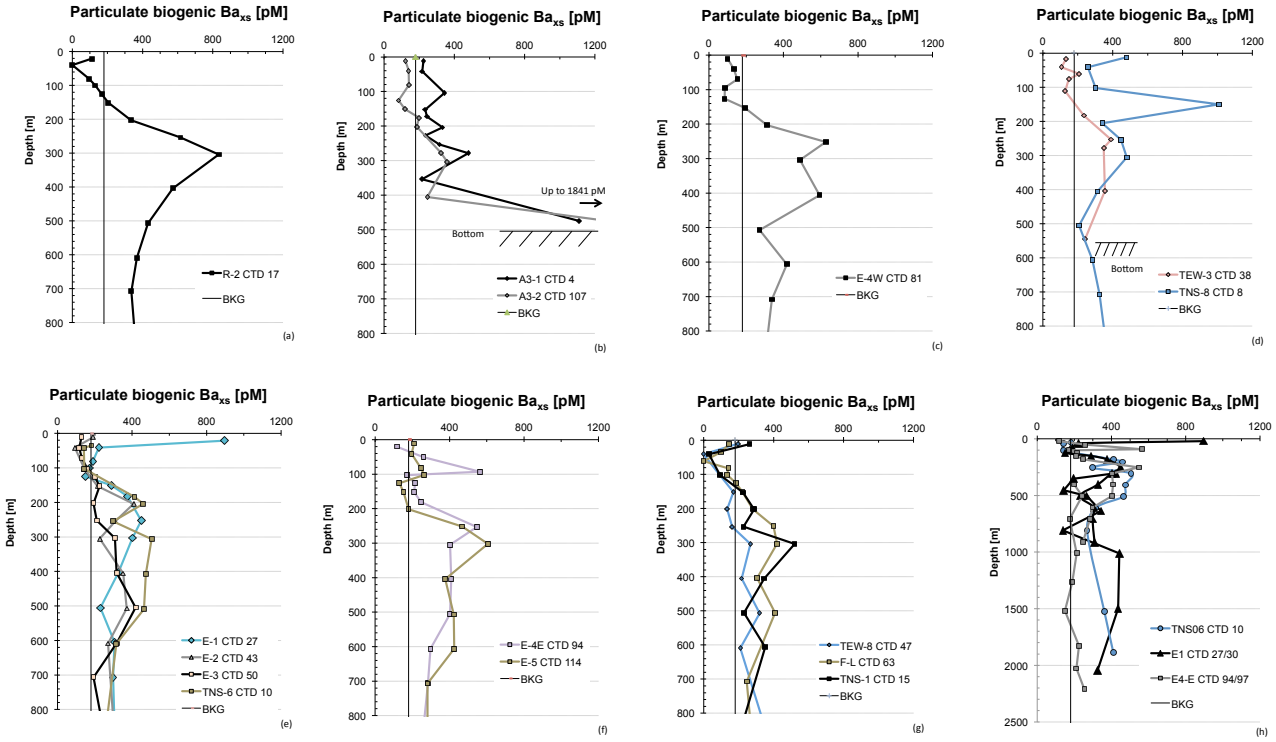
Particulate biogenic Ba$_{xs}$ [pM]
Depth [m]
R-2 CTD 17
BKG
(a)
Up to 1841 pM
Bottom
A3-1 CTD 4
A3-2 CTD 107
BKG
(b)
E-4W CTD 81
BKG
(c)
Bottom
TEW-3 CTD 38
TNS-8 CTD 8
BKG
(d)
E-1 CTD 27
E-2 CTD 43
E-3 CTD 50
TNS-6 CTD 10
BKG
(e)
E-4E CTD 94
E-5 CTD 114
BKG
(f)
TEW-8 CTD 47
F-L CTD 63
TNS-1 CTD 15
BKG
(g)
TNS06 CTD 10
E1 CTD 27/30
E4-E CTD 94/97
BKG
(h)

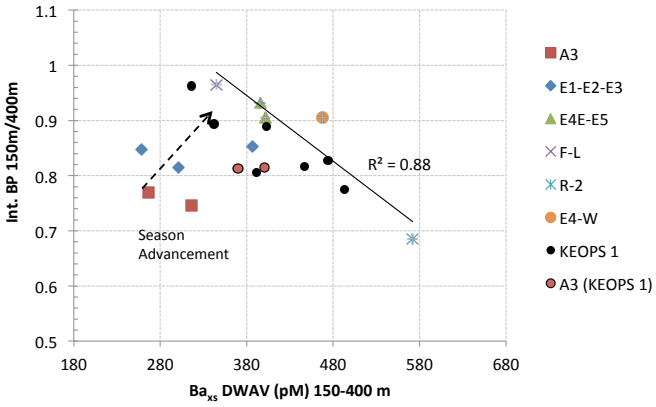
1.1
1
0.9
0.8
0.7
0.6
0.5
180
280
380
480
580
680
Int. BP 150m/400m
Ba$_{xs}$ DWAV (pM) 150-400 m
R² = 0.88
Season
Advancement
A3
E1-E2-E3
E4E-E5
F-L
R-2
E4-W
KEOPS 1
A3 (KEOPS 1)

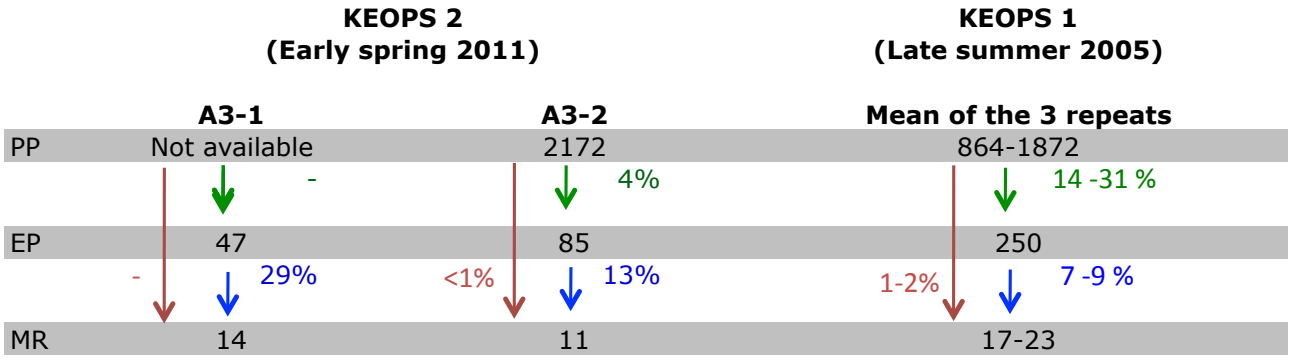

All fluxes in mgC m^{-2} d^{-1}
Blue values: r-ratio, mesopelagic remineralization efficiency (MR/EP)
Grenn values: EP/PP
Red values: MR/PP

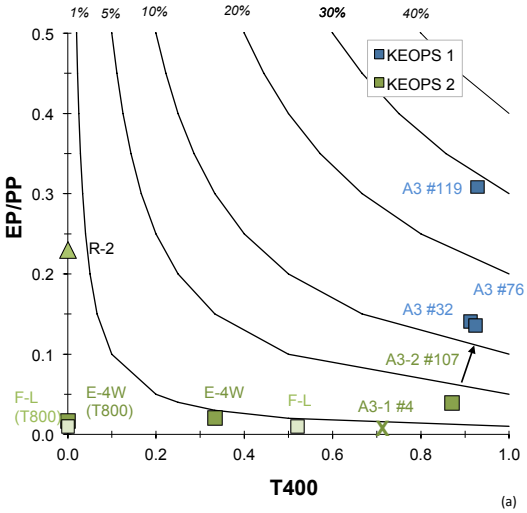
1%
5%
10%
20%
30%
40%
KEOPS 1
KEOPS 2
A3 #119
A3 #76
A3 #32
A3-2 #107
R-2
F-L
(T800)
E-4W
(T800)
E-4W
F-L
A3-1 #4
EP/PP
T400
0.0
0.1
0.2
0.3
0.4
0.5
0.6
0.8
1.0

(a)

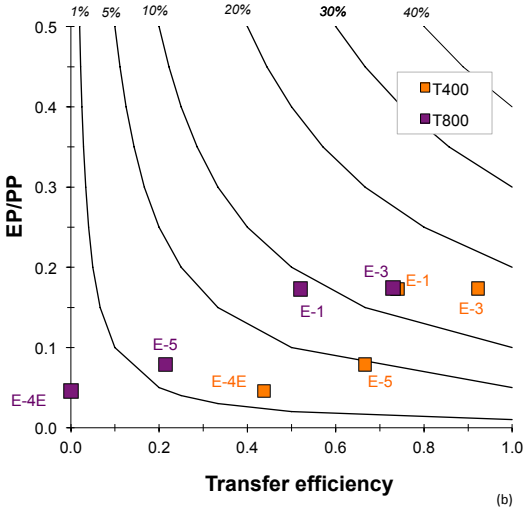
1%
5%
10%
20%
30%
40%
T400
T800
E-3
E-1
E-1
E-3
E-5
E-4E
E-5
E-4E
EP/PP
Transfer efficiency
0.0
0.1
0.2
0.3
0.4
0.5
0.6
0.8
1.0

(b)

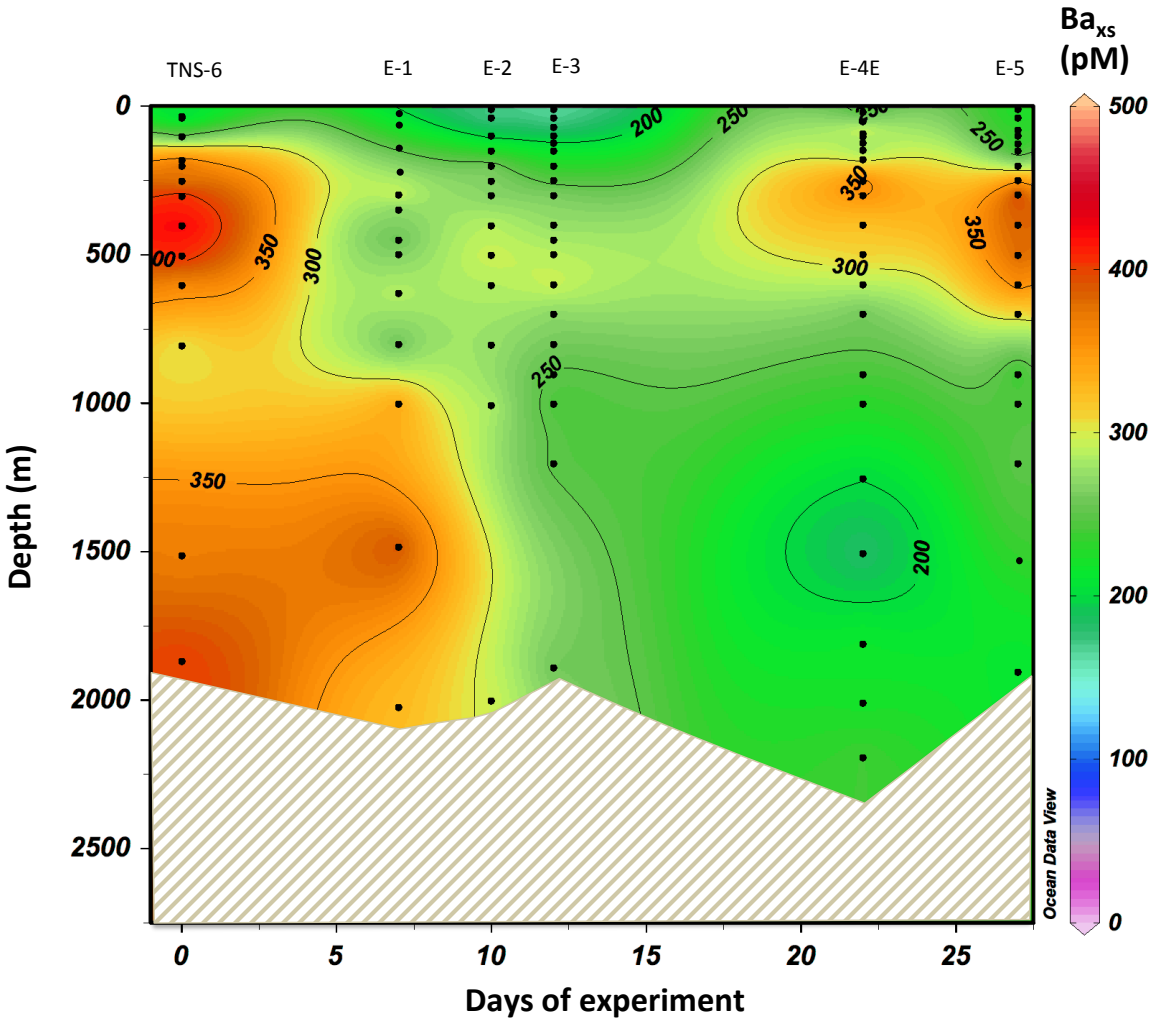
TNS-6
E-1
E-2
E-3
E-4E
E-5
Ba xs (pM)
Depth (m)
Days of experiment
Ocean Data View

Station	CTD cast #	Long (°E)	Lat (°S)	Date of sampling	Seafloor [m]	DWAv° Ba_{xs} [pM] 150- 400 m	DWAv Ba_{xs} [pM] 150- 800 m	MR°° 150- 400 m [mgC/m^2/d]	MR Stnd Uncertainty %	MR 150- 800 m [mgC/m^2/d]	MR Stnd Uncertainty %
Plateau											
A3-1	4*	72.080	50.629	20/10	530	316	/	14	4	/	/
A3-2	107*	72.056	50.624	16/11	527	267	/	11	5	/	/
TEW-3	38	71.018	48.799	31/10	560	324	/	28	8	/	/
Meander time series											
TNS-6	10	72.277	48.779	22/10	1885	427	389	31	7	69	17
E-1	27/30	72.187	48.458	29,30/10	2056	387	325	26	6	48	14
E-2	43	72.077	48.523	1/11	2003	301	309	15	5	42	13
E-3	50/55	71.967	48.702	03,04/11	1915	258	286	10	4	35	12
E-4E	94/97	72.563	48.715	13,14/11	2210	395	357	27	7	58	15
E-5	113/114	71.900	48.412	18/11	1920	402	380	28	7	66	17
Polar Front Zone											
TNS-1	15	71.501	46.833	23/10	2280	350	315	22	6	45	14
TEW-8	47	74.999	48.471	2/11	2786	199	240	2	4	20	11
F-L	63/68	74.659	48.532	06,07/11	2695	345	328	21	6	49	14
Polar Front											
E-4W	81/87	71.425	48.765	11,12/11	1384	468	411	36	8	76	18
Antarctic Zone											
R-2 (Reference site)	17/20	66.717	50.359	25,26/10	2300	572	456	50	10	91	20
TNS-8	8	72.240	49.463	21/10	1030	473	358	37	8	59	15

*Station A3 (CTD #4 and #107); integration up to 354 and 405 m
DWAV°= Depht weighted average value
MR°°= Mesopelagic C remineralization

Station	CTD	MLD [m]	Ez** [m]	PP° Ez [mgC/m^2/d]	EP°° 150 m [mgC/m2/d]	MR 150-400 m [mgC/m^2/d]	MR 150-800 m [mgC/m^2/d]	EP/PP	r-ratio 150-400 m	r-ratio 150-800 m	T400	T800
Plateau												
A3-1	4*	161	/	/	47	14	/	/	0.29	/	0.70	/
A3-2	107*	165	38	2172	85	11	/	0.04	0.13	/	0.87	/
Reference site												
R-2	17/20	111	92	132	30	50	91	0.23	1.65	3.02	0	0
Meander time series												
E-1	27/30	84	64	578	100	26	48	0.17	0.26	0.48	0.74	0.52
E-3	50/55	41	68	748	130	10	35	0.17	0.08	0.27	0.92	0.73
E-4E	94/97	77	34	1037	48	27	58	0.05	0.57	1.21	0.43	0.00
E-5	113/114	36	54	1064	84	28	66	0.08	0.33	0.78	0.67	0.22
Polar Front Zone												
F-L	63/68	21	29	3380	43	21	49	0.01	0.48	1.13	0.52	0
Polar Front												
E-4W	81/87	67	31	3287	54	36	76	0.02	0.67	1.41	0.33	0

*Station A3 (CTD4 and 107); MR integrated up to 354 and 405 m
**EZ euphotic layer (till 1% PAR level)
° PP data from Cavagna et al. (this issue)
°° EP data from PLanchon et al. (this issue)

Station A3

A3-1 CTD4

Niskin	Depth [m]	Ba_{xs} [pM]	Al [nM]
23	11	224	35
21	42	217	64
19	104	345	65
17	152	234	19
15	173	244	19
13	204	333	17
11	227	235	8
9	253	315	6
7	279	480	8
5	354	216	21
1	474	1108	155

A3-2 CTD 107

Niskin	Depth [m]	Ba_{xs} [pM]	Al [nM]
23	11	122	16
21	40	140	12
19	81	141	10
17	126	82	27
15	151	119	14
13	176	199	9
11	202	186	14
9	277	323	24
7	303	359	32
5	405	247	19
1	513	1842	186

Station RK2

R-2 CTD17

Niskin	Depth [m]	Ba_{xs} [pM]	Al [nM]
24	21	110	107
23	40	0	693
22	80	95	49
20	100	131	27
18	126	168	5
16	151	205	4
14	203	334	3
13	253	616	6
12	304	834	16
10	404	573	9
9	507	430	10
7	608	367	4
5	708	337	10
1	911	368	13

R-2 CTD 20

Niskin	Depth [m]	Ba_{xs} [pM]	Al [nM]
17	356	546	12
15	507	239	17
13	609	226	7
11	812	267	3
10	1011	189	2
8	1520	201	4
6	1832	184	2
1	2473	286	3

Station E

E-1 CTD 27

Niskin	Depth [m]	Ba_{xs} [pM]	Al [nM]
24	21	896	166
23	41	221	131
22	81	190	161
20	101	172	102
18	125	150	10
16	151	290	9
14	182	375	5
13	253	450	12
12	303	402	9
10	403	327	10
9	505	230	6
7	605	305	10
5	707	298	10
1	913	309	7

E-1 CTD 30

Niskin	Depth [m]	Ba_{xs} [pM]	Al [nM]
17	303	424	30
16	353	195	25
15	455	143	6
13	505	268	6
11	636	343	7
10	808	138	2
8	1011	442	4
6	1498	436	9
1	2042	326	7

E-2 CTD 43

Niskin	Depth [m]	Ba_{xs} [pM]	Al [nM]
23	11	192	43
21	41	93	152
18	102	143	17
16	153	215	57
14	204	408	9
12	254	311	6
10	305	227	4
8	406	353	5
7	507	371	9
6	609	271	10
5	813	297	14
4	1016	350	35
1	2020	302	11

E-3 CTD 50

Niskin	Depth [m]	Ba_{xs} [pM]	Al [nM]
24	11	129	45
23	42	117	93
22	71	130	28
20	102	160	22
18	125	201	11
16	153	225	18
14	203	193	3
13	252	210	2
12	304	309	6
10	404	316	7
9	505	419	64
7	606	320	14
5	707	193	12
1	912	265	5

Station E (continued)

E-3 CTD 55

Niskin	Depth [m]	Ba_{xs} [pM]	Al [nM]
17	404	185	5
16	455	272	5
15	505	176	6
13	605	378	5
11	810	258	3
10	910	172	2
8	1012	184	3
6	1214	228	6
1	1908	237	9

E-4W CTD 81

Niskin	Depth [m]	Ba_{xs} [pM]	Al [nM]
24	10	101	16
23	41	134	17
22	70	152	5
20	94	86	18
18	126	84	7
16	153	193	8
14	203	312	4
13	252	628	17
12	304	488	12
10	406	594	11
9	507	272	11
7	607	418	12
5	708	338	21
1	909	294	14

E-4W CTD 87

Niskin	Depth [m]	Ba_{xs} [pM]	Al [nM]
17	304	277	9
16	354	350	10
15	453	233	7
13	606	182	9
11	811	186	5
10	910	187	7
8	1011	268	61
6	1214	249	29
1	1384	250	30

E-4E CTD 94

Niskin	Depth [m]	Ba_{xs} [pM]	Al [nM]
24	20	116	32
23	51	260	11
22	93	563	223
20	103	170	5
18	126	215	9
16	152	210	6
14	181	247	7
13	253	547	4
12	305	403	78
10	404	408	26
9	505	403	26
7	606	298	13
5	706	285	8
1	912	245	65

Station E (continued)

E-4E CTD 97

Niskin	Depth [m]	Ba_{xs} [pM]	Al [nM]
21	404	199	2
18	505	242	3
13	706	175	1
8	1012	212	11
7	1265	189	2
6	1518	149	2
5	1827	225	43
4	2027	212	12
1	2212	254	9

E-5 CTD 113

Niskin	Depth [m]	Ba_{xs} [pM]	Al [nM]
10	911	111	3
8	1011	266	16
6	1214	256	15
1	1922	208	5

E-5 CTD 114

Niskin	Depth [m]	Ba_{xs} [pM]	Al [nM]
24	11	210	5
23	41	196	14
22	82	245	4
20	102	264	14
18	126	131	6
16	152	153	5
14	202	181	2
13	252	469	6
12	302	606	9
10	404	377	13
9	507	422	11
7	606	425	7
5	707	281	12
1	910	281	6

Transect West-East

TEW-3 CTD38

Niskin	Depth [m]	Ba_{xs} [pM]	Al [nM]
23	16	133	40
21	41	107	112
19	61	209	45
17	76	148	20
13	112	128	13
11	183	235	8
9	253	391	11
7	277	348	9
5	404	356	8
1	545	242	13

TEW-8 CTD 47

Niskin	Depth [m]	Ba_{xs} [pM]	Al [nM]
23	10	196	31
21	41	0	251
18	102	92	41
16	152	169	45
14	202	134	9
12	254	164	5
10	304	268	12
8	405	217	5
7	507	319	5
6	609	209	8
5	809	330	14
4	1011	334	22
1	2812	11179	826

Station F-L

F-L CTD 63

Niskin	Depth [m]	Ba_{xs} [pM]	Al [nM]
24	11	146	37
23	35	97	41
22	61	0	228
20	82	141	36
18	101	134	5
16	126	185	5
14	151	221	5
13	202	280	7
12	252	399	8
10	303	420	7
9	404	305	26
7	506	408	7
5	707	247	10
1	911	282	11

F-L CTD 68

Niskin	Depth [m]	Ba_{xs} [pM]	Al [nM]
17	405	264	6
16	456	233	9
15	506	339	12
13	607	265	3
11	910	718	7
10	1013	257	5
8	1215	316	8
6	1772	225	7
1	2741	2999	131

Transect North-South

TNS-1 CTD15

Niskin	Depth [m]	Ba_{xs} [pM]	Al [nM]
23	11	262	62
21	41	30	90
18	102	93	15
16	153	225	17
14	202	289	5
12	253	228	2
10	304	521	4
8	405	346	3
7	506	230	1
6	607	352	13
5	809	234	4
4	1520	127	6
1	2282	211	19

TNS-6 CTD 10

Niskin	Depth [m]	Ba_{xs} [pM]	Al [nM]
23	35	182	26
21	42	141	12
18	103	143	14
16	184	413	11
14	204	461	8
12	255	298	5
10	306	505	7
8	407	474	4
7	509	464	9
6	610	315	15
5	813	269	9
4	1526	362	13
1	1886	410	21

TNS-8 CTD8

Niskin	Depth [m]	Ba_{xs} [pM]	Al [nM]
23	12	478	45
21	41	258	53
18	102	303	32
16	150	1008	33
14	205	341	10
12	254	447	6
10	305	481	4
8	405	312	3
7	505	208	3
6	606	283	7
5	707	325	11
4	910	376	35
1	1000	294	28